

Representability of algebraic topology for biomolecules in machine learning based scoring and virtual screening

Zixuan Cang¹, Lin Mu², and Guo-Wei Wei^{1,3,4} *

¹ Department of Mathematics

Michigan State University, MI 48824, USA

² Computer Science and Mathematics Division

Oak Ridge National Laboratory, Oak Ridge, USA

³ Department of Biochemistry and Molecular Biology

Michigan State University, MI 48824, USA

⁴ Department of Electrical and Computer Engineering

Michigan State University, MI 48824, USA

August 29, 2017

Abstract

This work introduces a number of algebraic topology approaches, such as multicomponent persistent homology, multi-level persistent homology and electrostatic persistence for the representation, characterization, and description of small molecules and biomolecular complexes. Multicomponent persistent homology retains critical chemical and biological information during the topological simplification of biomolecular geometric complexity. Multi-level persistent homology enables a tailored topological description of inter- and/or intra-molecular interactions of interest. Electrostatic persistence incorporates partial charge information into topological invariants. These topological methods are paired with Wasserstein distance to characterize similarities between molecules and are further integrated with a variety of machine learning algorithms, including k-nearest neighbors, ensemble of trees, and deep convolutional neural networks, to manifest their descriptive and predictive powers for chemical and biological problems. Extensive numerical experiments involving more than 4,000 protein-ligand complexes from the PDBBind database and near 100,000 ligands and decoys in the DUD database are performed to test respectively the scoring power and the virtual screening power of the proposed topological approaches. It is demonstrated that the present approaches outperform the modern machine learning based methods in protein-ligand binding affinity predictions and ligand-decoy discrimination.

Contents

I	Introduction	3
II	Methods and algorithms	5
II.A	Persistent homology	5
II.A.1	Simplicial complex	5
	Simplex	5
	Simplicial complex	5
II.A.2	Homology	5
	Chain	5
	Boundary operator	5
	Cycle group	6
	Boundary group	6
	Homology group	6

*Address correspondences to Guo-Wei Wei. E-mail:wei@math.msu.edu

	Betti number	6
II.A.3	Persistent homology	6
	Filtration	6
	Persistence	6
II.A.4	Simplicial complexes and filtration	6
	Vietoris-Rips complex	6
	Alpha complex	6
II.B	Biological considerations	6
	Covalent bonds	6
	Non-covalent interactions	6
	Multi-leveled protein structures	7
	Protein-ligand, protein-protein, and protein-nucleic acid complexes	7
II.C	Element specific persistent homology	7
II.D	Distance matrix induced persistent homology	7
II.D.1	Multi-level persistent homology	8
II.D.2	Interactive persistent homology	9
II.D.3	Correlation function based persistent homology	9
	Flexibility and rigidity index based filtration matrix	9
II.D.4	Electrostatic persistence	10
II.D.5	Multicomponent persistent homology	10
II.E	Feature generation from topological invariants	10
	Counts in bins	10
	Barcode statistics	11
	Persistence diagram slice and statistics	11
	2D representation	11
II.F	Machine learning algorithms	13
II.F.1	K-nearest neighbors algorithm via barcode space metrics	13
	Bottleneck distance metric	13
	Wasserstein metric	13
II.F.2	Gradient boosting trees	13
II.F.3	Deep convolutional neural networks	13
III	Results and discussion	14
III.A	Ligand based protein-ligand binding affinity prediction	15
	Data set	15
	Feature vectors for gradient boosting trees	15
	Barcode space metrics for k-nearest neighbor regression	16
	Performance of multicomponent persistent homology	16
	Robustness of topological models	16
III.B	Complex based protein-ligand binding affinity prediction	18
	Data sets	18
	Groups of topological features and their performance in association with GBT	19
	Robustness of GBT algorithm against redundant element combination features and potential overfitting	19
	Usefulness of more than 2 element types for interactive Betti-0 barcodes	21
	Importance of atomic charge information	21
	Relevance of elements that are rare with respect to the data sets	21
	2D persistence for deep convolutional neural networks	22
III.C	Structure-based virtual screening	23
	DUD data set	23
	Data processing	23
	Evaluation	23
	Topology based machine learning models	24

Arguably, machine learning has become one of the most important developments in data science and artificial intelligence. With its ability to extract features of various levels hierarchically, deep convolutional neural networks (CNNs) have made breakthroughs in image processing, video, audio, and computer vision,^{1,2} whereas recurrent neural networks have found success in analyzing sequential data, such as text and speech.³⁻⁶ Deep learning algorithms are able to automatically extract high-level features and discover intricate patterns in large data sets. In general, one of major advantages of machine learning algorithms is their ability to deal with large data sets and uncover complicated relationships.

Recently, machine learning has become an indispensable tool in biomolecular data analysis and structural bioinformatics. Almost every computational problem in molecular biophysics and biology, such as the predictions of solvation free energy, solubility, partition coefficient, protein-ligand binding affinities, mutation induced protein stability change, molecular multipolar electrostatics, virtual screening etc, has machine learning based approaches that are either parallel or complementary to their physics based counterparts. The success of deep learning has fueled the rapid growth in several areas of biological science,^{3,5,6} including bioactivity of small-molecule drugs⁷⁻¹⁰ and genetics,^{11,12} where large data sets are available.

Despite the success of deep CNNs in dealing with small molecules, the direct application of deep CNNs to three-dimensional (3D) macromolecule structures is extremely expensive and prone to accuracy reduction due to insufficient grid resolution and inadequate chemical labeling.¹³ As a result, deep CNNs have not been as competitive in terms of accuracy and efficiency as other commonly used machine learning algorithms, such random forest and gradient boosted trees, for predictions based on 3D biomolecular data. A major obstacle in the development of deep learning nets for 3D biomolecular data is the presence of geometric and biological complexities.

Biomolecules can be characterized by geometric features, electrostatic features, high level features, and amino-acid sequence features based on physical, chemical and biological understandings.¹⁴ Geometric features, such as coordinates, distances, angles, surface areas¹⁵⁻¹⁷ and curvatures,¹⁸⁻²¹ are important descriptors of biomolecules.²²⁻²⁴ However, geometric features often involve too much structural detail and are frequently computationally intractable for large biomolecular data sets. Electrostatic features include atomic partial charges, Coulomb potentials, atomic electrostatic solvation energies, and polarizable multipolar electrostatics.²⁵ These descriptors become essential for highly charged biomolecular systems, such as nucleic acid polymers and some protein-ligand complexes. High level features refer to pKa values of ionizable groups and neighborhood amino acid compositions, such as the involvement of hydrophobic, polar, positively charged, negatively charged, and special case residues. Sequence features consist of secondary structures, position-specific scoring matrix (PSSM), and co-evolution information. Sequence features and annotations provide a rich resource for bioinformatics analysis of biomolecular systems. Topology offers a new unconventional representation of biomolecules. Topological features for biomolecules can be generated in a variety of ways.²⁶ Some of the most powerful topological features are obtained from multicomponent persistent homology, or element specific persistent homology (ESPH).^{14,27} Recently, we carried out a comprehensive comparison of the performance of geometric features, electrostatic features, high level features, sequence features and topological features, for the prediction of mutation induced protein folding free energy changes of four mutation data sets.¹⁴ Surprisingly, topological features outperform all the other features.¹⁴

Unlike geometry, topology is well known for its power of simplification to geometric complexity.²⁸⁻³⁵ The global description generated by classical topology is based on the concept of neighborhood. If a space can be continuously deformed to another, they are considered to present the same topological features. In this sense, topology can not distinguish between a folded protein and its unfolded form. Such property prevents the use of classical topology for the characterization of biomolecular structures. Instead of using topology to describe a single configuration of connectivity, persistent homology scans over a sequence of configurations ordered by a filtration parameter and output a sequence of topological invariants, which partially captures part of geometric features. Persistent homology has been applied to biomolecular systems in our earlier works.

In mathematics, persistent homology is a relatively new branch of algebraic topology.^{29,36} When dealing with proteins and small molecules, it is conventionally to consider atoms as point clouds. For a given point cloud data set, one type of persistent homology turns each point into a sphere with their radii systematically increasing. The corresponding topological invariants and their persistence over the varying radius values can be computed. Therefore, this method embeds multiscale geometric information into topological invariants to achieve

an interplay between geometry and topology. Consequently, persistent homology captures topological structures continuously over a range of spatial scales. It is called persistent homology because at each given radius, topological invariants, i.e., Betti numbers, are practically calculated by means of homology groups. In the past decade, much theoretical formulation³⁷⁻⁴⁶ and many computational algorithms⁴⁷⁻⁵² have been developed. One-dimensional (1D) topological invariants generated from persistent homology is often visualized by persistence barcodes^{53,54} and persistence diagrams.⁵⁵ In recent years, multidimensional persistence has attracted much attention^{43,56} in hope that it can better characterize the data shape when there are multiple measurements of interest.

Persistent homology has been applied to various fields, including image/signal analysis,⁵⁷⁻⁶² chaotic dynamics verification,^{63,64} sensor networks,⁶⁵ complex networks,^{66,67} data analysis,⁶⁸⁻⁷² shape recognition⁷³⁻⁷⁵ and computational biology.^{76,77,77-79} Compared with traditional computational topology⁸⁰⁻⁸² and/or computational homology, persistent homology inherently adds an additional dimension, i.e., the filtration parameter. The filtration parameter can be used to embed important geometric or quantitative information into topological invariants. As such, the importance of retaining geometric information in topological analysis has been recognized,⁸³ and persistent homology has been advocated as a new approach for handling big data sets.^{54,68,84-86} Recently, we have introduced persistent homology for mathematical modeling and prediction of nano-particles, unfolding proteins and other biomolecules.^{26,87} We proposed the molecular topological fingerprint (TF) to reveal topology-function relationships in protein folding and protein flexibility.²⁶ We established some of the first quantitative topological analyses in our persistent homology based predictions of the curvature energy of fullerene isomers.^{87,88} We have also shown correlation between persistence barcodes and energies computed with physical models during molecular dynamics experiments.²⁶ Moreover, we have introduced the first differential geometry based persistent homology that utilizes partial differential equations (PDEs) in filtration.⁸⁸ Most recently, we have developed a topological representation to address additional measurements of interest, by stacking the persistent homology outputs from a sequence of frames in molecular dynamics or a sequence of different resolutions.^{89,90} We have also introduced the first use of topological fingerprints for resolving ill-posed inverse problems in cryo-EM structure determination.⁹¹ In 2015, we constructed one of the first topology based machine-learning algorithms in protein classification involving tens of thousands of proteins and hundreds of tasks.⁹² We also developed persistent-homology based software for the automatic detection of protein cavities and binding pockets.⁹³

Despite of much success, it was found that persistent homology has a limited characterization power for proteins and protein complexes, when applied directly to a single selection of atoms.⁹² Essentially, biomolecules are not only complex in their geometric constitution, but also intricate in biological constitution. In fact, the biological constitution is essential to biomolecular structure and function. Persistent homology that is designed to reduce the geometric complexity of a biomolecule can easily miss biological information. To overcome this difficulty, we have introduced multicomponent persistent homology or element specific persistent homology (ESPH) to recognize the chemical constitution during the topological simplification of biomolecular geometric complexity.^{14,27,94} In ESPH, the atoms of a specific set of element types in a biomolecule are selected so that certain chemical information is emphasized. Our ESPH is not only able to outperform other geometric and electrostatic representations in large data sets, but is also able to shed light on the molecular mechanism of protein-ligand binding, such as the relative importance of hydrogen bond, hydrophilicity and hydrophobicity at various spatial ranges.²⁷

The objective of the present work is to further explore the representability and reduction power of multicomponent persistent homology for biomolecules. To this end, we take a combinatorial approach to scan a variety of element combinations and examine the characterization power of these components. Additionally, we also propose a multi-level persistence to study the topological properties of non-covalent bond interactions. This approach enables us to devise persistent homology to describe the interactions of interest between atoms that are connected by a series of covalent bonds, and delivers richer representation especially for small molecules. Moreover, to enhance the power of topological representation, we introduce electrostatic persistence, which embeds charge information in topological invariants, as a new class of features in multicomponent persistent homology. Electrostatics are of paramount importance in biomolecules. The aforementioned approaches can be realized via the modification of the distance matrix with a more abstract setting, for example, Vietoris-Rips complex. The complexity reduction is guaranteed in the 1D topological representation of 3D biomolecular structures. Obviously, the multicomponent persistent homology representation of biomolecule leads to a higher machine learning dimensionality compared to the original single component persistent homology for a biomolecule. Therefore, it is subject to overfitting or overlearning problem in machine learning theory. Fortunately, gradient boosting trees (GBT) method is relatively insensitive to redundant high dimensional topological features.¹⁴ Finally, since com-

ponents can be arranged as a new dimension ordered by their feature importance, multicomponent persistent homology barcodes are naturally a two-dimensional (2D) representation of biomolecules. Such a 2D representation can be easily used as image-like input data in a deep CNN architecture, with different topological dimensions, i.e., Betti-0, Betti-1, and Betti-2, being treated as multichannels. Such approach addresses the nonlinear interactions among important element combinations while keeping the information from less important ones. Barcode space metrics, such as bottleneck distance and more generally, Wasserstein metrics,^{95,96} offer a direct description of similarity between molecules and can be readily used with nearest neighbor regression or kernel based methods. The performance of Wasserstein distance for protein-ligand binding affinity predictions is examined in this work.

The rest of this manuscript is organized as follows. Section II is devoted to introduce methods and algorithms. We present multicomponent persistent homology, multi-level interactive persistent homology, vectorized persistent homology representation and electrostatic persistence. These formulations are crucial for the representability of persistent homology for biomolecules. Machine learning algorithms associated with the present topological data analysis are briefly discussed. Results are presented in Section III. We first consider the characterization of small molecules. More precisely, the cross-validation of protein-ligand binding affinities prediction via solely ligand topological fingerprints is studied. We illustrate the excellent representability of our multicomponent persistent homology by a comparison with physics based descriptors. Additionally, we investigate representational power of the proposed topological method on a few sets of benchmark protein-ligand binding data sets, namely, PDBBind v2007, PDBBind v2013, PDBBind v2015 and BPDBBind v2016.⁹⁷ These data sets contain thousands of protein-ligand complexes and have been extensively studied in the literature. Results indicate that multicomponent persistent homology offers one of most powerful representations of protein-ligand binding systems. The aforementioned study of the characterization of small molecules and protein-ligand complexes leads to an optimal selection of features and models to be used for virtual screening. Finally, we consider the directory of useful decoys (DUD) database to examine the representability of our multicomponent persistent homology for virtual screening to distinguish actives from decoys. The DUD data set used in this work has a total of about 100000 compounds containing 2950 active ligands, which bind to 40 targets from six families. A large number of state-of-the-art virtual screening methods have been applied to this data set. We demonstrate that the present multicomponent persistent homology outperforms all other methods. This paper ends with a conclusion.

II Methods and algorithms

II.A Persistent homology

The concept of persistent homology is built on the mathematical concept of homology, which associates a sequence of algebraic objects, such as abelian groups, to topological spaces. For discrete data such as atomic coordinates in biomolecules, algebraic groups can be defined via simplicial complexes, which are constructed from simplices, generalizations of the geometric notion of nodes, edges, triangles and tetrahedrons to arbitrarily high dimensions. Homology characterizes the topological connectivity of geometric objects in terms of topological invariants, i.e., Betti numbers, which are used to distinguish topological spaces by counting k -dimensional holes. Betti-0, Betti-1 and Betti-2, respectively, represent independent components, rings and cavities in a physical sense. In persistent homology, Betti numbers are evaluated along with a filtration parameter, such as the radius of a ball or the level set of a hypersurface function, that continuously varies over an interval. Therefore, persistent homology is induced by the filtration. For a given biomolecule, the change and the persistence of topological invariants over the filtration offer a unique characterization. These concepts are very briefly discussed below.

II.A.1 Simplicial complex

Simplex A k -simplex denoted by σ^k is the convex hull of $k + 1$ affinely independent points in \mathbb{R}^k . The convex hull of each nonempty subset of the $k + 1$ points forms a subsimplex and is regarded as a *face* of σ^k . The points are also called *vertices* of σ^k .

Simplicial complex A set of simplices K is a *simplicial complex* if all faces of any simplex in K are also in K and the intersection of any pair of simplices in K is either empty or a common face of the two simplices.

II.A.2 Homology

Chain A k -chain of a simplicial complex K denoted by $C_k(K)$ is the formal linear combination of all the k -simplices in K . Here, we take the \mathbb{Z}_2 field for the coefficients of the linear combination. Under the rule of fields, a k -chain is a group called *chain group*.

Boundary operator A *boundary operator* denoted by $\partial_k : C_k(K) \rightarrow C_{k-1}(K)$ maps a linear combination of k -simplices to the same linear combination of the boundaries of the k -simplices. With a k -simplex $\sigma^k = [v_0, \dots, v_k]$

where v_i are the vertices of σ^k , the *boundary operator* is defined as $\partial_k \sigma^k = \sum_{i=0}^k \sigma_i^{k-1}$, where σ_i^{k-1} is a $(k-1)$ -simplex which is a face of σ^k with the i th vertex being absent.

Cycle group A k -cycle is a k -chain whose image under the *boundary operator* ∂_k is the empty set. The collection of all the k -cycles forms a group denoted by $Z_k(K)$ which is the kernel of $\partial_k : C_k(K) \rightarrow C_{k-1}(K)$.

Boundary group The image of $\partial_k + 1 : C_{k+1}(K) \rightarrow C_k(K)$ is called the boundary group and is denoted by B_k . B_k is a subgroup of Z_k following the property of the *boundary operator* that $\partial_k \circ \partial_{k+1} = 0$.

Homology group The k th *homology group* is the quotient group defined as $H_k = Z_k/B_k$. It is used to compute Betti numbers.

Betti number The k th *Betti number* β_k is defined and often computed as $\text{rank} H_k = \text{rank} Z_k - \text{rank} B_k$.

II.A.3 Persistent homology

Filtration A *filtration* of a *simplicial complex* K is a nested sequence of subcomplexes of K such that $\emptyset = K^0 \subset K^1 \subset \dots \subset K^m = K$. Each K^i is itself a *simplicial complex*.

Persistence Given a *simplicial complex* K with its filtration K^i , the p -persistent k th *homology group* of K^i is defined as $H_k^{i,p} = Z_k^i / (B_k^{i+p} \cap Z_k^i)$.

II.A.4 Simplicial complexes and filtration

Given a finite set of points X and a non-negative scale parameter r , the Vietoris-Rips complex and alpha complex are constructed as follows.

Vietoris-Rips complex With a predefined metric $d(\cdot, \cdot)$ in X , a subset X' of X forms a simplex if $d(x_i, x_j) \leq r$ for all $x_i, x_j \in X'$. The collection of all such simplices is the Vietoris-Rips complex of the finite metric space X with scale parameter r denoted by $Rips(X, r)$. It is obvious that $Rips(X, r) \subseteq Rips(X, r')$ for $r \leq r'$.

Alpha complex With $Alpha(X, r)$ being the alpha complex of X with the scale parameter r and given the Delaunay triangulation induced by the Voronoi diagram of X , a simplex in the Delaunay triangulation belongs to $Alpha(X, r)$ if all its 1 -faces (1 -simplex as subset of the simplex) have length no greater than $2r$. Similar to Rips complex, alpha complex also has the property that $Alpha(X, r) \subseteq Alpha(X, r')$ for $r \leq r'$.

II.B Biological considerations

The development of persistent homology was motivated by its potential in the dimensionality reduction, abstraction and simplification of biomolecular complexity.³⁶ In the early applications of persistent homology to biomolecules, emphasis was given on major or global features. Short barcodes were regarded noise. For example, persistent homology was used to identify the tunnel in a Gramicidin A channel³⁶ and to study membrane fusion.⁹⁸ For the predictive modeling of biomolecules, features of a wide range of scales might all be important to the target quantity.²⁶ In the global scale, the biomolecular conformation should be captured. In the intermediate scale, the smaller intradomain cavities need to be identified. In the most local scale, the important substructures should be addressed, such as the pyrrolidine in the side chain of proline. These features of different scales can be reflected by barcodes with different centers and persistences. Therefore, applications in biomolecules can make a more exhaustive use of persistent homology,^{26,87} compared to some other applications where only global features matter while most local features are mapped to noise. Earlier use of persistent homology was focused on qualitative analysis. Only recently had persistent homology been devised as a quantitative tool.^{26,87} While the aforementioned applications are descriptive and regression based analysis, we have also applied persistent homology to predictive modeling of biomolecules.⁹² However, biomolecules are both structurally and biologically complex. Their geometric and biological complexities include covalent bonds, non-covalent interactions, effects of chirality, cis and trans distinctions, multi-leveled protein structures, and protein-ligand and protein-nucleic acid complexes. Covering a large range of spatial scales is not enough for a power model. The biological details should also be explored. We address the underlying biology and physics by modifying the distance function and selecting various sets of atoms according to element types, to describe different interactions. Some biological considerations are discussed in this section.

Covalent bonds Covalent bonds are formed via shared electron pairs or bonding pairs. The lengths and the number of covalent bonds can be easily detected from Betti-0 barcodes. For macromolecules, the same type of covalent bonds have very similar bond lengths and thus Betti-0 barcode patterns.

Non-covalent interactions Non-covalent interactions play a critical role in maintaining the 3D structure of biomolecules and mediating chemical and biological processes, such as solvation, partition coefficient, binding, protein-DNA specification, molecular self-assembly, etc. Physically, non-covalent interactions are due to electrostatic, van der Waals forces, hydrogen bonds, π -effects, hydrophobic effects, etc. The ability to characterize non-covalent interactions is an essential task in any methodological development. Betti-1 and Betti-2

barcodes are suitable for the characterization of the arrangement of such interactions in a larger scale. Additionally, we propose multi-level persistence and electrostatic persistence to reveal local and pairwise non-covalent interactions via Betti-0 barcodes as well.

Multi-leveled protein structures Protein structures are typically described in terms of primary, secondary, tertiary and quaternary ones. The protein primary structure is the linear sequence of amino acids in the polypeptide chain. A secondary structure mainly refers to α -helix and β -sheets, which are highly regular and can be easily detected by distinct Frenet-Serret frames. A tertiary structure refers to the 3D structure of a single polypeptide chain. Its formation involves various non-covalent interactions, salt bridges, hydration effects, and often disulfide bonds. A quaternary structure refers to the aggregation of two or more individual polypeptide chains into a 3D multiprotein complex. Protein structures are further complicated by its functional domains, motifs, and particular folds. The protein structural variability and complexity result in the challenge and opportunity for methodological developments. Various persistent homology techniques, including multicomponent, multi-level, multidimensional,⁹⁹ multiresolution,⁹⁰ electrostatic, and interactive²⁷ persistent homologies have been designed either in our earlier work or in this paper for protein structural variability and complexity.

Protein-ligand, protein-protein, and protein-nucleic acid complexes Topological characterization of proteins is further complicated by protein interactions or binding with ligands (drugs), proteins, DNA and/or RNA molecules. Although a normal protein involves only carbon (C), hydrogen (H), nitrogen (N), oxygen (O) and sulfur (S) atoms, its protein-ligand complexes bring a variety of other elements into the play, including, phosphorus (P), fluorine (F), chlorine (Cl), Bromine (Br), iodine (I), and many important biometals, such as calcium (Ca), potassium (K) sodium (Na), iron (Fe), copper (Cu), cobalt (Co), zinc (Zn), manganese (Mn), chromium (Cr), vanadium (V), tin (Sn), and molybdenum (Mo). Each biological element has important biological functions and its presence in biomolecules should be treated uniformly as a set of points in the point cloud data. The interaction of protein and nucleic acids can be very intricate. Qualitatively, multiscale and multi-resolution persistent homology demonstrates interesting features in 3D DNA structures.⁸⁹ Typically, 3D RNA structures are more flexible and difficult to extract topological patterns. Interactive persistent homology, element specific persistent homology and binned representation for persistent homology outputs were designed to deal with interactions between protein-ligand, protein-protein, and protein-nucleic acid complexes.^{14,27,94} These approaches worked well in protein-mutation site interactions.¹⁴ Additionally, multi-level persistent homology and electrostatic persistence proposed in this work are useful tools to describe some other specific interactions.

II.C Element specific persistent homology

One important issue is how to protect chemical and biological information during the topological simplification. As mentioned early, one should not treat different types of atoms as structureless points in a point cloud data. To this end, element specific persistent homology or multi-component persistent homology has been proposed to retain biological information in topological analysis.^{14,27,94} The element selection is similar to a predefined vertex color configuration for graphs.

When all atoms are passed to persistent homology algorithms, the information extracted mainly reflects the overall geometric arrangement of a biomolecule at different spatial scales. By passing only atoms of certain element types or of certain roles to the persistent homology analysis, different types of interactions or geometric arrangements can be revealed. In protein-ligand binding modeling, the selection of all carbon atoms characterizes the hydrophobic interaction network whilst the selection of all nitrogen and/or oxygen atoms characterizes hydrophilic network and the network of potential hydrogen bonds. In the protein structural analysis, computation on all atoms can identify geometric voids inside the protein which may suggest structural instability and computation on only C_α atoms reveals the overall structure of amino acid backbones. In addition, combination of various selections of atoms based on element types provides very detailed description of the biomolecular system and hidden relationships from the structure to function can then be learned by machine learning algorithms. This may lead to the discovery of important interactions not realized as *a priori*. This can be realized by passing the set of atoms of the selected element types to the persistent homology computation. This concept is used with the various definitions of distance matrix discussed as follows.

II.D Distance matrix induced persistent homology

Biomolecular systems are not only complex in geometry, but also in chemistry and biology. To effectively describe complex biomolecular systems, it is necessary to modify the filtration process. There are three commonly used filtrations, namely, radius filtration, distance matrix filtration, and density filtration, for biomolecules.^{26,90} A distance matrix defined with smoothed cutoff functions was proposed in our earlier work to deal with interactions within a spatial scale of interest in biomolecules.²⁶ In the present work, we introduce more distance matrices

to enhance the representational power of persistent homology and to cover some important interactions that were not covered in our earlier works. The distance matrices can be used with a more abstract construction of simplicial complexes, such as Vietoris-Rips complex.

II.D.1 Multi-level persistent homology

Small molecules such as ligands in protein-ligand complexes usually contain fewer atoms than large biomolecules such as proteins. Bonded atoms stay closer than non-bonded ones in most cases. As a result, the collection of Betti-0 bars will mostly provide the information about the length of covalent bonds. It is difficult to capture non covalent bond interactions among atoms especially hydrogen bonds and van der Waals pairwise interactions in Betti-0 barcodes. In order to describe non covalent interactions, we propose multi-level persistent homology, by simply modifying the distance matrix, similar to the idea of modifying distance matrix to emphasize on the interactions between protein and ligand.²⁷ Given the original distance matrix $\mathbf{M} = (d_{ij})$ with $1 \leq i, j \leq N$, the modified distance matrix is defined as

$$\widetilde{\mathbf{M}}_{ij} = \begin{cases} d_{\infty}, & \text{if atoms } i \text{ and } j \text{ are bonded,} \\ \mathbf{M}_{ij}, & \text{otherwise,} \end{cases} \quad (1)$$

where d_{∞} is a large number which is set to be greater than the maximal filtration value chosen by a persistent homology algorithm. Note that this matrix may fail to satisfy triangle inequality whilst still satisfies the construction principle of Rips complex.

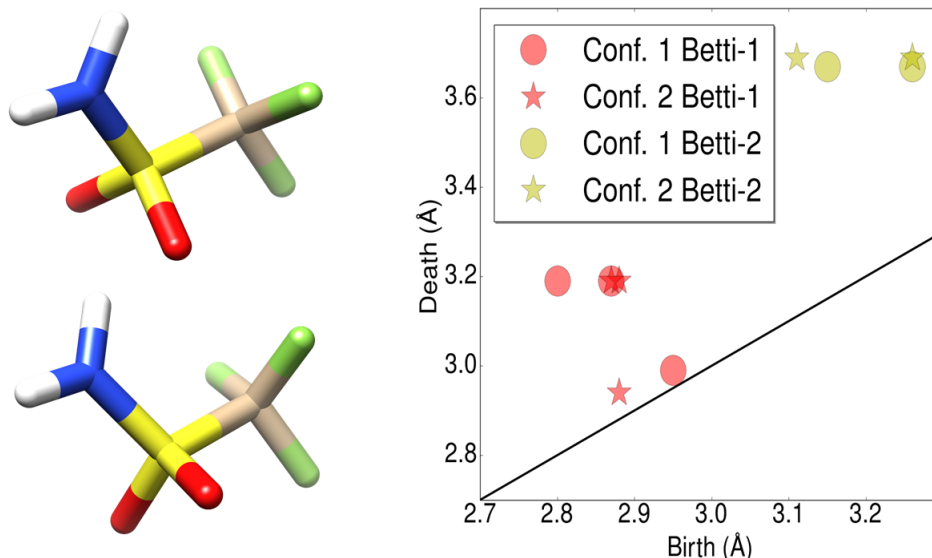


Figure 1: Illustration of representation ability of $\widetilde{\mathbf{M}}$ in reflecting structural perturbations among conformations of the same molecule. **a.** The structural alignment of two conformations of the ligand in protein-ligand complex (PDB:1BCD). **b.** The persistence diagram showing the Betti-1 and Betti-2 results generated using Rips complex with $\widetilde{\mathbf{M}}$ for two conformations. It is worth noticing that the barcodes generated using Rips complex with \mathbf{M} are identical for the two conformations.

The present multi-level persistent homology is able to describe any selected interactions of interest and delivers two benefits in characterizing biomolecules. Firstly, the pairwise non-covalent interactions can be reflected by Betti-0 barcodes. Secondly, such treatment generates more higher dimensional barcodes and the small structural fluctuation among different conformations of the same molecule can be captured. The persistent barcode representation of the molecule can be significantly enriched to better distinguish between different molecular structures and isomers. As an illustration, we take the ligand from the protein-ligand complex with PDB code "1BCD" which only has 10 atoms. A different conformation of the ligand is generated by using the Frog2 server.¹⁰⁰ The persistent barcodes generated using Rips complex with the distance matrices \mathbf{M} are identical and only have Betti-0 bars due to the simple structure. In this case, Betti-0 bars only reflect the length of each bond and therefore fail to distinguish two slightly different conformations of the same molecule. However, when the modified distance matrices $\widetilde{\mathbf{M}}$ are employed, the barcode representation is significantly enriched and is able to capture the tiny structural perturbation between conformations. An illustration of the outcome from the modified

distance matrix $\widetilde{\mathbf{M}}$ is shown in Figure 1. A general n th level persistence characterization of molecules can be obtained with the distance matrix $\widetilde{\mathbf{M}}^n$ as,

$$\widetilde{\mathbf{M}}_{ij}^n = \begin{cases} d_\infty, D(i, j) \leq n \\ \mathbf{M}_{ij}, \text{ otherwise,} \end{cases} \quad (2)$$

where $D(i, j)$ is the smallest number of bonds to travel from atom i to atom j and d_∞ is some number greater than the maximal filtration value.

II.D.2 Interactive persistent homology

In protein-ligand binding analysis and/or mutation analysis, we are interested in the change of topological invariants induced by binding interactions and/or mutations. Similar to the idea of multi-level persistent homology, we can design a distance matrix to focus on the interactions of interest. For a set of atoms, $A = A_1 \cup A_2$ with $A_1 \cap A_2 = \emptyset$ where only interactions between atoms from A_1 and atoms from A_2 are of interest.²⁷ The interactive distance matrix $\widehat{\mathbf{M}}$ is defined as

$$\widehat{\mathbf{M}}_{ij} = \begin{cases} \mathbf{M}_{ij}, \text{ if } a_i \in A_1, a_j \in A_2 \text{ or } a_i \in A_2, a_j \in A_1, \\ d_\infty, \text{ otherwise,} \end{cases} \quad (3)$$

where \mathbf{M} is the original distance matrix induced from Euclidean metrics or other correlation function based distances, a_i and a_j are atoms i and j , and d_∞ is a number greater than the maximal filtration value. In applications, A_1 and A_2 can be respectively sets of atoms of the protein and set of atoms of the ligand in a protein ligand complex. In this case, the characterization of interactions between ligand and protein is an important task. In the modeling of site specific mutation induced protein stability changes, A_1 could be the set of atoms at the mutation site and A_2 could be the set of atoms of surrounding residues close to the mutation site. Similar treatment can be used for protein-protein and protein-nucleic acid interactions.

II.D.3 Correlation function based persistent homology

For biomolecules, the interaction strength between pair of atoms usually does not align linearly to their Euclidean distances. For example, van der Waals interaction is often described by the Lennard-Jones potential. Therefore, kernel function filtration can be used to emphasize certain geometric scales. Correlation function based filtration matrix was introduced in our earlier work:²⁶

$$\bar{\mathbf{M}}_{ij} = 1 - \Phi(d_{ij}, \eta_{ij}), \quad (4)$$

where $\Phi(d_{ij}, \eta_{ij})$ is a radial basis function and η_{ij} is a scale parameter. This filtration can be incorporated in the element specific persistent homology

$$\hat{\mathbf{M}}_{ij} = \begin{cases} d_\infty, \text{ if atom } i \text{ or atom } j \in \mathcal{U}, \\ 1 - \Phi(d_{ij}, \eta_{ij}), \text{ otherwise.} \end{cases} \quad (5)$$

Additionally, one can simultaneously use two or more correlation functions characterized by different scales to generate a multiscale representation of biomolecules.¹⁰¹

Flexibility and rigidity index based filtration matrix One form of the correlation function based filtration matrix is constructed by flexibility and rigidity index. In this case, the Lorentz function is used in Eq. (5)

$$\Phi(d_{ij}; \eta_{ij}, \nu) = \frac{1}{1 + \left(\frac{d_{ij}}{\eta_{ij}}\right)^\nu}, \quad (6)$$

where d_{ij} is the Euclidean distance between point i and point j and η_{ij} is a parameter controlling the scale and is related to radius of two atoms. When distance matrices based on such correlation functions are used, patterns at different spatial scales can be addressed separately by altering the scale parameter η_{ij} . Note that the rigidity index is given by¹⁰²

$$\mu_i = \sum_j \Phi(d_{ij}; \eta_{ij}, \nu). \quad (7)$$

This expression is closely related to the rigidity density based volumetric filtration.⁹⁰

II.D.4 Electrostatic persistence

Electrostatic effects are some of the most important effects in biomolecular structure, function and dynamics. The embedding of electrostatics in topological invariants is of particular interest and can be very useful in describing highly charged biomolecules such as nucleic acids and their complexes. We introduce electrostatics interaction induced distance functions in Eq. (8) to address the electrostatic interactions among charged atoms. The abstract distance between two charged particles are rescaled according to their charges and their geometric distance, and is modeled as

$$\Phi(d_{ij}, q_i, q_j; c) = \frac{1}{1 + \exp(-cq_i q_j / d_{ij})}, \quad (8)$$

where d_{ij} is the distance between the two atoms, q_i and q_j are the partial charges of the two atoms, and c is a nonzero tunable parameter. c is set to a positive number if opposite charge interactions are to be addressed and is set to a negative number if like charge interactions are of interest. The form of the function is adopted from sigmoid function which is widely used as an activation function in neural networks. Such function regularizes the input signal to the $[0, 1]$ interval. Other functions can be similarly used. This formulation can be extended to systems with dipole or higher order multipole approximations to electron density. The weak interactions due to long distances or neutral charges result in correlation values close to 0.5. When $c > 0$, the repulsive interaction and attractive interaction deliver the correlation values in $(0.5, 1)$ and $(0, 0.5)$ respectively. The distances induced by $\Phi(d_{ij}, q_i, q_j; c)$ are used to characterize electrostatic effects. The parameter c is rather physical but chosen to effectively spread the computed values over the $(0, 1)$ interval so that the results can be used by machine learning methods. Another simple choice of charge correlation functions is

$$\Phi(d_{ij}, \eta_{ij}, q_i, q_j) = q_i q_j \exp(-d_{ij} / \eta_{ij}).$$

However, this choice will lead to a different filtration domain. Additionally, a charge density can be constructed

$$\mu^c(\mathbf{r}) = \sum_j q_j \exp(-\|\mathbf{r} - \mathbf{r}_j\| / \eta_j), \quad (9)$$

where \mathbf{r} is a position vector, $\|\mathbf{r} - \mathbf{r}_j\|$ is the Euclidean distance between \mathbf{r} and j th atom position \mathbf{r}_j and η_j is a scale parameter. Equation (9) can be used for electrostatic filtration as well. In this case, the filtration parameter can be the charge density value and cubical complex based filtration can be used.

II.D.5 Multicomponent persistent homology

Multicomponent persistent homology refers to the construction of multiple persistent homology components from a given object to describe its properties. Obviously, element specific persistent homology leads to multicomponent persistent homology. Nevertheless, in element specific persistent homology, the emphasis is given to the appropriate selection of important elements for describing certain biological properties or functions. For example, in biological context, electronegative atoms are selected for describing hydrogen bond interactions, polar atoms are selected for describing hydrophilic interactions, and carbon atoms are selected for describing hydrophobic interactions. Note that in chemical context, an atom may have many sharply different chemical and physical properties, depending on its oxidation states. Whereas, in multicomponent persistent homology, the emphasis is placed on the systematic generation of topological invariants from different combinatorial possibilities and the construction of 2D or high-dimensional persistent maps for deep convolutional neural networks. Additionally, multicomponent persistent homology can also be constructed from the combination of other persistences, such as electrostatic persistent homology, resolution induced persistent homology, etc.

II.E Feature generation from topological invariants

Barcode representation of topological invariants offers a visualization of persistent homology analysis. In machine learning analysis, one needs to convert the barcode representation of topological invariants into machine learning feature vectors. To this end, we introduce two methods, i.e., counts in bins and barcode statistics, to generate feature vectors from sets of barcodes. These methods are discussed below.

Counts in bins For a given set of atoms A , we denote its barcodes as $\mathbf{B} = \{I_\alpha\}_{\alpha \in A}$ and characterize each bar by an interval $I_\alpha = [b_\alpha, d_\alpha]$, where b_α and d_α are respectively the birth and death positions on the filtration axis. The length of each bar, or the persistence of topological invariant is given by $p_\alpha = d_\alpha - b_\alpha$. To locate the position position of all bars and persistences, we further split the set of barcodes on the filtration axis into a predefined N bins $\mathbf{Bin} = \{rmBin_i\}_{i=1}^N$ where $\text{Bin}_i = [l_i, r_i]$, where l_i and r_i are the left and the right positions of the i th bin.

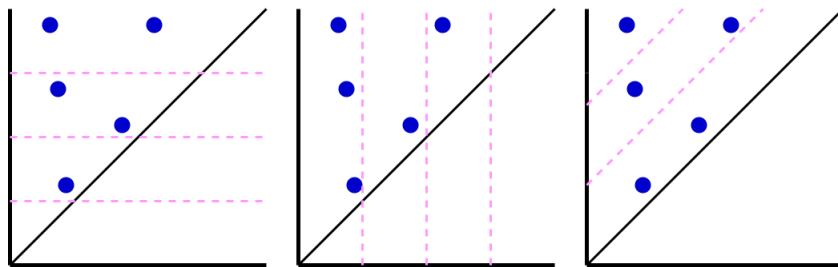


Figure 2: Illustration of dividing set of barcodes into subsets. The barcodes are plotted as persistence diagrams with the horizontal axis being birth and the vertical axis being death. From left to right, the subsets are generated according to the slicing of death, birth, and persistence values.

We generate features by counting the numbers of births, deaths, and persistences in each bin, which leads to three counting feature vectors, namely, counts of birth F_b^C , death F_d^C , and persistence F_p^C ,

$$\begin{aligned}
 F_{b,i}^C(\mathbf{B}) &= \|\{[b_\alpha, d_\alpha] \in \mathbf{B} | l_i \leq b_\alpha \leq r_i\}\|, 1 \leq i \leq N, \\
 F_{d,i}^C(\mathbf{B}) &= \|\{[b_\alpha, d_\alpha] \in \mathbf{B} | l_i \leq d_\alpha \leq r_i\}\|, 1 \leq i \leq N, \\
 F_{p,i}^C(\mathbf{B}) &= \|\{[b_\alpha, d_\alpha] \in \mathbf{B} | b_\alpha \leq r_i \text{ or } l_i \leq d_\alpha\}\|, 1 \leq i \leq N,
 \end{aligned} \tag{10}$$

where $\|\cdot\|$ is number of elements in a set. Note that the above discussion should be applied to three topological dimensions, i.e., barcodes of Betti-0 (\mathbf{B}^0), Betti-1 (\mathbf{B}^1) and Betti-2 (\mathbf{B}^2). In general, this approach enables the description bond lengths, including the length of non-covalent interactions, in biomolecules and is referred as binned persistent homology in our earlier work^{14,27,94}

Barcode statistics Another method of feature vector generation from a set of barcodes is to extract important statistics of barcode collections such as maximum values and standard deviations. Given a set of bars $\mathbf{B} = \{[b_\alpha, d_\alpha]\}_{\alpha \in A}$, we define sets of **Birth** = $\{b_\alpha\}_{\alpha \in A}$, **Death** = $\{d_\alpha\}_{\alpha \in A}$, and **Persistence** = $\{d_\alpha - b_\alpha\}_{\alpha \in A}$. Three statistic feature vectors F_b^S , F_d^S , and F_p^S can then be generated in the sense of the statistics of the collection of barcodes. For example, F_b^S consists of $\text{avg}(\mathbf{Birth})$, $\text{std}(\mathbf{Birth})$, $\text{max}(\mathbf{Birth})$, $\text{min}(\mathbf{Birth})$, $\text{sum}(\mathbf{Birth})$, and $\text{cnt}(\mathbf{Birth})$, where $\text{avg}(\cdot)$ is the average value of a set of numbers, $\text{std}(\cdot)$ is the standard deviation of a set of numbers, $\text{max}(\cdot)$ and $\text{min}(\cdot)$ are maximum and minimum values in a set of numbers, $\text{sum}(\cdot)$ is the summation of elements in a set of numbers, and $\text{cnt}(\cdot)$ is the count of elements in a set. The generation of F_d^S is the same by examining the set **Death**. F_p^S contains the same information with two extra terms, the birth and death values of the longest bar. Statistic feature vectors are collected from barcodes of three topological dimensions, i.e., Betti-0, Betti-1 and Betti-2.

Persistence diagram slice and statistics A more thorough description of sets of barcodes is to first divide the sets into subsets and extract features analogously to the *barcode statistics* method. As shown in Figure 2, a persistence diagram can be divided into slices in different directions. The barcodes that fall in each slice form a subset. Each subset is described in terms of feature vector by using the *barcode statistics* method. When the persistence diagram is sliced horizontally, members in each subset have similar death values and the barcode statistics feature vector is generated for the set of birth values. Similarly, members in each subset have similar birth values if the persistence diagram is sliced vertically, and the barcode statistics feature vector is generated for the set of death values. The barcode statistics feature vectors are generate for both set of birth values and set of death values if the persistence diagram is sliced diagonally, where members in each subset have similar persistence. This type of feature vector generation describes the set of barcodes in more detail but will produce long feature vectors.

2D representation The construction of multi-dimensional persistence is an interesting topic in persistent homology. In general, it is believed that multi-dimensional persistent has better representational power for complex systems described by multiple parameters.⁴³ Although multidimensional persistence is hard to compute, one can compute persistence for one parameter while fixing the rest of the parameters to a sequence of fixed values. In the case where there are two parameters, a bifiltration can be done by taking turns to fix one parameter to a sequence of fixed values while computing persistence for the other parameter. For example, one can take a sequence of resolutions and compute persistence for distance with each fixed resolution. The sequence of outputs can be stacked to form a multidimensional representation.⁹⁹

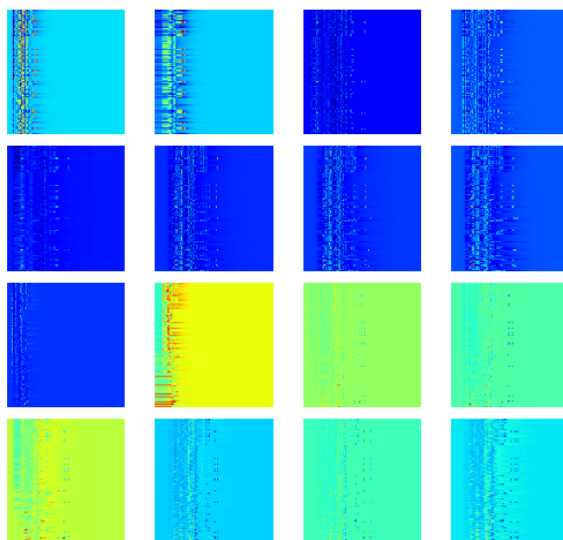


Figure 3: The 2D topological maps of the 16 channels of sample 1wkm in PDBBind. The top 8 maps are for protein-ligand complex and the other 8 maps are for the difference between protein-ligand complex and protein only. For each map, the horizontal axis is the dimension of spatial scale and the vertical axis is element combinations ordered by their importance.

Computing persistence multiple times and stacking the results is especially useful when the parameters that are not chosen to be the filtration parameter are naturally discrete with underlying orders. For example, the multicomponent or element specific persistent homology will result in many persistent homology computations over different selections of atoms. These results can be ordered by the percentage of atoms used of the whole molecule or by their importance in classical machine learning methods. Also, multiple underlying dimensions exist in the element specific persistent homology characterization of molecules. This property enables 2D or 3D topological representation of molecules. Based on the observation that the performance of the predictor degenerates when too many element combinations are used, we order the element combinations according to their individual performance on the task using methods of ensemble of trees. Combining the dimension of spatial scale and dimension of element combinations, a 2D topological representation is obtained. Such representation is expected to work better in the case of complex geometry such as protein-ligand complexes. With $\mathbf{E} = \{E_j\}_{j=1}^{N_E}$ denoting the collection of element combinations ordered by their individual performance on the task and $\mathbf{B}^{dim}(E_i)$ being the Betti- dim barcodes obtained with atoms of element combination E_j , eight 2D representations are defined as

$$\{F_{d,i}^C(\mathbf{B}^0(E_j)), F_{p,i}^C(\mathbf{B}^0(E_j)), F_{b,i}^C(\mathbf{B}^1(E_j)), F_{d,i}^C(\mathbf{B}^1(E_j)), F_{p,i}^C(\mathbf{B}^1(E_j)), F_{b,i}^C(\mathbf{B}^2(E_j)), F_{d,i}^C(\mathbf{B}^2(E_j)), F_{p,i}^C(\mathbf{B}^2(E_j))\}_{i=1, \dots, N}^{j=1, \dots, N_E}, \quad (11)$$

where $F_{\gamma,i}^C$ with $\gamma = b, d, p$ is the barcode counting rule defined in Eq. (10). For Betti-0, since all bars start from zero, there is no need for $F_{b,i}^C(\mathbf{B}^0(E_j))$. These eight 2D representations are regarded as eight channels of a 2D topological image. In protein-ligand binding analysis, 2D topological features are generated for the barcodes of a protein-ligand complex and for the differences between barcodes of the protein-ligand complex and those of the protein. Therefore, we have a total of 16 channels in a 2D image for the protein-ligand complex. This 16-channel image can be fed into the training or the prediction of convolutional neural networks.

In the characterization of protein-ligand complexes using alpha complexes, 2D features are generated from the alpha complex based on persistent homology computations of protein and protein-ligand complex. A total of 128 element combinations are considered. The $[0, 12]\text{\AA}$ interval is divided into 120 equal length bins, which defines the resolution of topological images. Therefore, the input feature for each sample is a $120 \times 128 \times 16$ tensor. Figure 3 illustrates 16 channels of sample 1wkm in PDBBind database. These images are directly used in deep convolutional neural networks for training and prediction.

II.F Machine learning algorithms

We discuss three machine learning algorithms, including k-nearest neighbors (KNN) regression, gradient boosting trees and deep convolutional neural networks.

II.F.1 K-nearest neighbors algorithm via barcode space metrics

One of the simplest machine learning algorithms is k-nearest neighbors (KNN) for classification or for regression. In KNN regression, for a given object, its property values is obtained by the average or the weighted average of the values of its k nearest neighbors induced by the given metric. Then, the problem becomes how to construct a metric on the dataset.

In the present work, instead of constructing feature vectors from sets of barcodes, the similarity between biomolecules can simply be derived from distances between sets of barcodes generated from different biomolecules. Popular barcode space metrics include the bottleneck distance induced metric¹⁰³ and more generally, the Wasserstein metrics.^{95,96} The definition of the two metrics is summarized as follows.

Bottleneck distance metric Given two bars $I_1 = [b_1, d_1]$ and $I_2 = [b_2, d_2]$ regarded as ordered pairs in \mathbb{R}^2 , the l^∞ distance between the two bars is defined as $\Delta(I_1, I_2) = \max(|b_2 - b_1|, |d_2 - d_1|)$. For a single bar $I = [b, d]$, $\lambda(I)$ is defined as $\lambda(I) = (d - b)/2$ which helps reflect the difference between the existence of the bar itself and the void. For two finite sets of barcodes $\mathbf{B}_1 = \{I_\alpha^1\}_{\alpha \in A}$ and $\mathbf{B}_2 = \{I_\beta^2\}_{\beta \in B}$ and a bijection θ from $A' \subseteq A$ to $B' \subseteq B$, the penalty of θ is defined as

$$P(\theta) = \max(\max_{\alpha \in A'}(\Delta(I_\alpha^1, I_{\theta(\alpha)}^2)), \max_{\alpha \in A-A'}(\lambda(I_\alpha^1)), \max_{\beta \in B-B'}(\lambda(I_\beta^2))). \quad (12)$$

Intuitively, a bijection θ is penalized for linking two bars with large difference and for ignoring long bars from either set. The bottleneck distance is defined as $d^\infty(I^1, I^2) = \min_{\theta} P(\theta)$, where the minimum is taken over all possible bijections from subsets of A to subsets of B .

Wasserstein metric The Wasserstein metric, a L_p generalized analog to the bottleneck distance can be defined with the penalty⁹⁶

$$P^p(\theta) = \sum_{\alpha \in A'} \Delta(I_\alpha^1, I_{\theta(\alpha)}^2)^p + \sum_{\alpha \in A-A'} \lambda(I_\alpha^1)^p + \sum_{\beta \in B-B'} \lambda(I_\beta^2)^p \quad (13)$$

and the corresponding distance $d^p(\mathbf{B}_1, \mathbf{B}_2) = (\min_{\theta} P^p(\theta))^{\frac{1}{p}}$. It reduces to the bottleneck distance by setting $p = \infty$. In this work, we choose $p = 2$.

Wasserstein metric measures the closeness of barcodes generated from different biomolecules. It will be interesting to consider other distances for metric spaces, such as Hausdorff distance, Gromov-Hausdorff distance,¹⁰⁴ and Yau-Hausdorff distance¹⁰⁵ for biomolecular analysis. However, an exhaustive study of this issue is beyond the scope of the present work.

The barcode space metrics can be directly used to assess the representation power of various persistent homology methods on biomolecules without potential overfitting effects induced by manually generated feature vectors. We show in the section of results that the barcode space metrics induced similarity measurement is significantly correlated to molecule functions.

Wasserstein metric measures from biomolecules can also be directly implemented in a kernel based method such as nonlinear support vector machine algorithm for classification and regression tasks. However, this aspect is not explored in the present work.

II.F.2 Gradient boosting trees

Gradient boosting trees is an ensemble method which ensembles individual decision trees to achieve the capability of learning complex feature target maps and can effectively prevent overfitting by using shrinkage technique. The gradient boosting trees method is implemented using the GradientBoostingRegressor module in scikit-learn software package.¹⁰⁶ A set of parameters found to be efficient in our previous study on the protein-ligand binding affinity prediction²⁷ is used uniformly unless specified. The parameters used are $n_estimators=20000$, $max_depth=8$, $learning_rate=0.005$, $loss='ls'$, $subsample=0.7$, $max_features='sqrt'$.

II.F.3 Deep convolutional neural networks

A widely used convolutional neural network architecture is employed beginning with convolution layers followed by dense layers. Due to the limited computation resources, parameter optimization is not performed, while most parameters are adopted from our earlier work.⁹⁴ Reasonable parameters are assigned manually. The detailed architecture is shown in Figure 4. The Adam optimizer with learning rate 0.0001 is used. The loss function is the mean squared error function. The network is trained with a batch size of 32 and 500 epochs. The training data

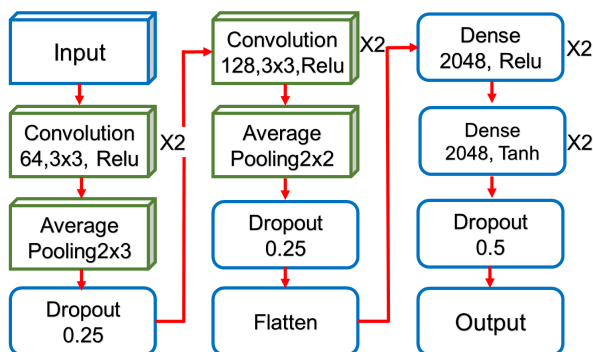


Figure 4: The architecture of the deep convolutional neural network. The structured layers are shown in boxes and the unstructured layers are shown in rectangles. The convolution layers are drawn with number of filters, filter size, and activation function. The dense layers are drawn with number of neurons and activation function. The pooling size of the pooling layers and dropout rate of the dropout layers are listed. The layers that are repeated twice are marked with "x2" sign on the right side of the layer.

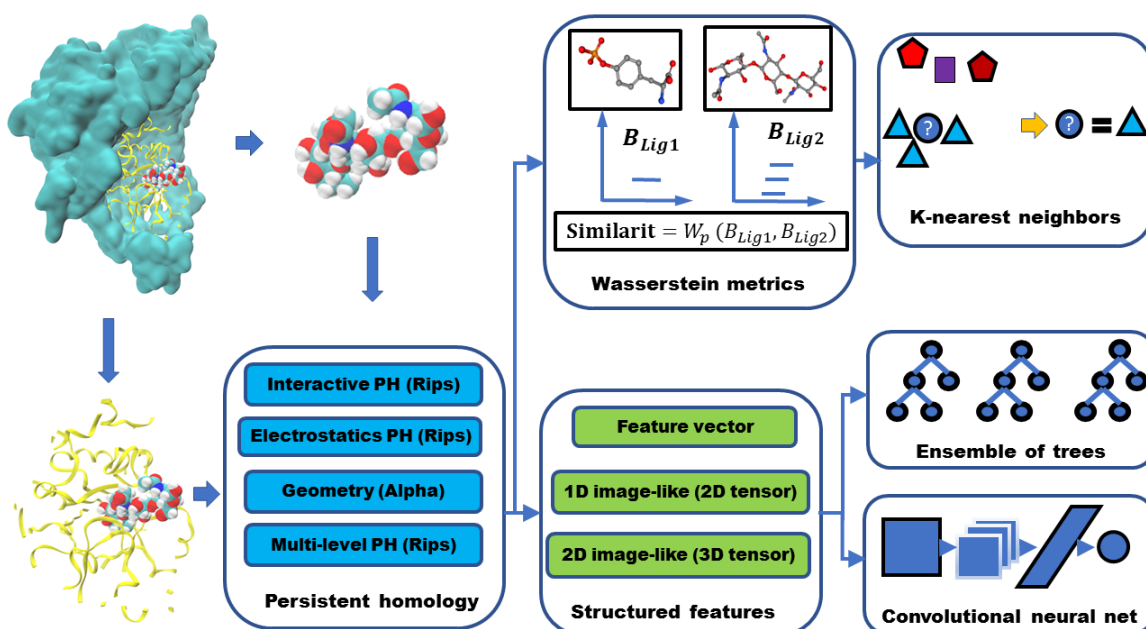


Figure 5: An illustration of the topology based machine learning algorithms used scoring and virtual screening.

is shuffled for each epoch. The deep convolutional neural network is implemented using Keras¹⁰⁷ with Theano backend.¹⁰⁸

III Results and discussion

Rational drug design and discovery have rapidly evolved into some of the most important and exciting research fields in medicine and biology. These approaches potentially have a profound impact on human health. The ultimate goal is to determine and predict whether a given drug candidate will bind to a target so as to activate or inhibit its function, which results in a therapeutic benefit to the patient. Virtual screening is an important process in rational drug design and discovery which aims to identify actives of a given target from a library of small molecules. There are mainly two types of screening techniques, ligand-based and structure-based. Ligand-based approach depends on the similarity among small molecule candidates. Structure-based approach tries to dock a candidate molecule to the target protein and judge the candidate with the modeled binding affinity based on the docking poses. In structure-based screening, knowledge based rescoring methods using machine learning or deep learning approaches have shown improvements when applied on top of docking algorithms.^{109–111} We also apply our method as a rescoring machine to rerank the candidates based on docking poses generated by docking software.

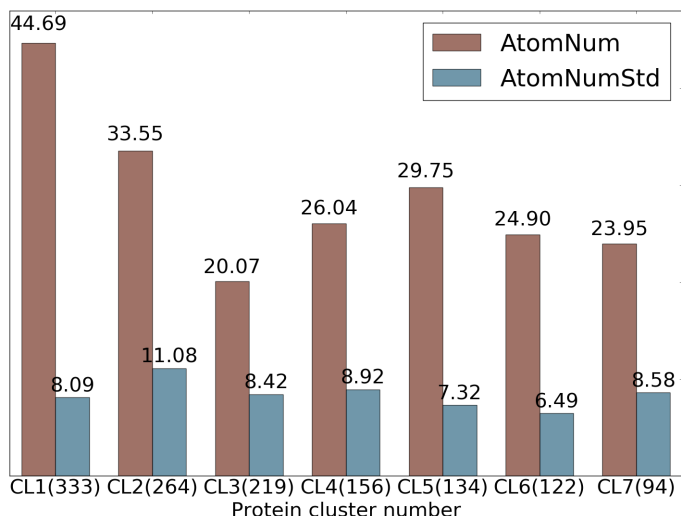


Figure 6: Statistics of ligands in 7 protein clusters in S1322. The average numbers of heavy atoms of a ligand in each protein cluster are shown in red and the standard deviations of number of heavy atoms across each protein cluster are shown in blue. The number of ligands in each cluster is given in parentheses.

This section explores the representational power of the proposed persistent homology methods for the prediction of protein-ligand binding affinities and the discrimination of actives and non-actives for protein targets. To this end, we use the present method to investigate three types of problems. First, we consider a ligand based protein-ligand binding affinity predictions. This problem is designed to examine the representability of the proposed topological methods for small molecules. Additionally, we study protein-ligand complex based binding affinity prediction. This problem enables us to understand the capability of the proposed topological methods for dealing with protein-ligand complexes. Finally, we examine the complex based classification of active ligands and non-active decoys, i.e., structure-based virtual screening (VS). The optimal selection of features and methods are determined by studying the first two applications and this leads to the main application studied in this work, the topological structure-based virtual screening. Computational algorithms used in this study are illustrated in Fig. 5.

III.A Ligand based protein-ligand binding affinity prediction

We consider the protein-ligand binding affinity prediction using a ligand based approach. Essential hypothesis is that, for a given binding site on a target protein, similar ligands or ligands with similar decisive substructures have similar binding free energies. One data set and two machine learning algorithms, i.e., gradient boosting trees and KNN with Wasserstein metrics are employed in this study to analyze the representational power of the proposed method. Cross-validations within the ligand set of each protein target are carried out.

Data set To assess the representational ability of the present persistent homology algorithms on small molecules, we use a high quality data set of 1322 protein-ligand complexes with binding affinity data involving 7 protein clusters introduced earlier (denoted as S1322).¹¹² It is a subset of the PDDBind v2015 refined set and its detail is given in the Supporting Material of Ref.¹¹² We consider a ligand based approach to predict the binding affinities of protein-ligand complexes in various protein clusters. As such, only the ligand information is used in our topological analysis. The ligand structures are taken from PDDBind database without modification. Numbers of ligands in protein clusters range from 94 to 333. Statistics of the data set in terms of the average number of heavy atoms and its standard deviations is given in Fig. 6. In this dataset, cluster 1 has a relatively large binding site that is able to accommodate large ligands, while cluster 3 has a relatively small binding site.

Feature vectors for gradient boosting trees In this test, Rips complex based and alpha complex based persistent homology computations up to Betti-2 are performed for a variety of atom collections with different element types using the Euclidean metric and multi-level distance defined in Eq. 1. Two types of features are generated and are denoted by F^C , which is a combination of F_b^C , F_d^C , and F_p^C , and F^S , which is a combination of F_b^S , F_d^S , and F_p^S . For sets of Betti-0 bars, only F_d^C and F_d^S are computed. In each protein cluster, 10-fold or 5-fold cross

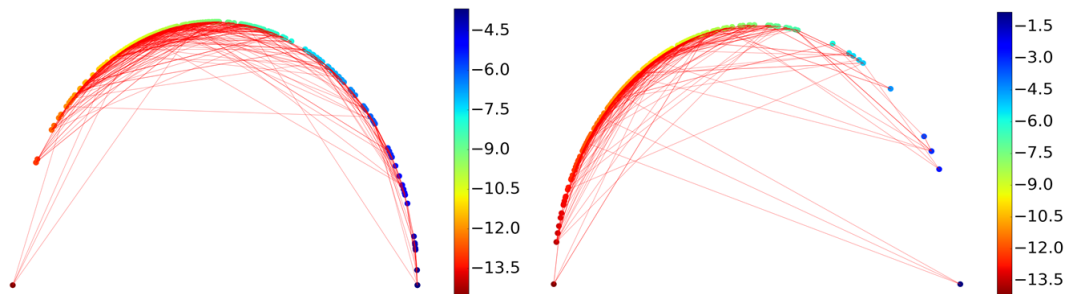


Figure 7: An illustration of similarities between ligands measured by their barcode space Wasserstein distances. Ligands are ordered according to their binding affinities and are represented as dots on the semicircle. Each dot is connected with two nearest neighbors based on their barcode space Wasserstein distances. An optimal prediction would be achieved if lines stay close to the semicircle. The majority of the connections stay near the boundary to the upper half sphere demonstrating that barcode space metric based Wasserstein distance measurement reflects the similarity in function, i.e., the binding affinity in this case. The protein clusters with the best and the worst performance are shown. (a) Protein cluster 2. (b) Protein cluster 3.

validation is repeated 20 times for each subset of feature vectors depending on selected element type. The median Pearson correlation coefficients and the root-mean-square error (RMSE) in kcal/mol are reported. For Rips complex, both level 0 computation with distance matrix \mathbb{M} and level 1 computation with distance matrix $\widetilde{\mathbb{M}}^1$ as defined in Eq. (2) are performed. A comparison of these results is shown in Table S2. The results corresponding to alpha complex are shown in Table S1. %reftab:alpha. The average performance for alpha complex and Rips complex has a Pearson correlation coefficient of 0.987.

Barcode space metrics for k-nearest neighbor regression The barcodes generated using Rips complex with distance matrices \mathbb{M} and $\widetilde{\mathbb{M}}^1$ are collected and the distance between each pair of sets of barcodes are measured using the Wasserstein metric d^2 . Leave-one-out prediction for every sample is performed with k-nearest neighbor regression with $k = 3$ within each protein cluster based on the Wasserstein metric. The results are shown in Table S3. The performance of the best performing and the worst performing protein clusters is shown in Figure 7. The better the performance, the closer the lines are to the semicircle.

The experiments done for this section are summarized in Table 1.

Performance of multicomponent persistent homology It can be noticed from Table 2 that topological features generated from barcode statistics typically outperform those created from counts in bins. R-B012-E-S-GBT and R-B012-M1-S-GBT perform similarly in the majority of the protein clusters whilst R-B012-M1-S-GBT which is based on $\widetilde{\mathbb{M}}^1$ significantly outperforms R-B012-E-S-GBT which is based on Euclidean distance in protein cluster 3 and 6. To assess in what circumstances does the multi-level persistent homology improve the original persistent homology characterization of small molecules, we analyze the statistics of the size of ligands in Figure 6. It turns out that protein cluster 3 has the smallest average number of heavy atoms and protein cluster 6 has the smallest standard deviation of the number of heavy atoms. This observation partially answers the question that in the cases where the small molecules are relatively simple and are relatively of similar size, multi-level persistent homology is able to enrich the characterization of the small molecules which further improves the robustness of the model. Such enrichment or improvement over the original persistent homology approach is mainly realized in higher dimensional Betti numbers, i.e. Betti-1 and Betti-2. In Table 2, the results with ID through 7 to 12 confirm that the Betti-0 features from computation with $\widetilde{\mathbb{M}}^1$ are inferior to the results with Euclidean distance whilst the Betti-1 or Betti-2 features based on $\widetilde{\mathbb{M}}^1$ outperforms the best result with Euclidean distance in most cases.

It is interesting to note that although Wasserstein metric based KNN methods are not as accurate as GBT approaches, the consensus result obtained by averaging over various Wasserstein metric predictions is quite accurate. Unlike GBT approaches, Wasserstein metric utilizes only one type of barcodes. In fact, R-B0-E-KNN, R-B1-M1-KNN and R-B2-M1-KNN work very well.

Finally, FFT-BP 5-fold cross validation results were obtained based on multiple additive regression trees and a set of physical descriptors, including geometry charge, electrostatics and van der Waals interactions for S1322.¹¹² Since multiple additive regression trees are essentially the same as the GBT used in the present work, it is appropriate to compare the FFT-BP results with the GBT results in this work. The current topological descriptors built on only ligands have more predictive power than the physical descriptors built on protein-ligand complexes constructed in our earlier work.¹¹²

Experiment	Description
A-B012-E-C-GBT	The barcodes are generated using alpha complex on different sets of atoms based on different element combinations. The features are constructed using Betti-0, Betti-1, and Betti-2 barcodes following the <i>counts in bins</i> method with bins equally dividing the interval [0, 5]. Here 32 different element combinations are considered, including {C, N, O, S, CN, CO, CS, NO, NS, OS, CNO, CNS, COS, NOS, CNOS, CNOSPFCIBrI, H, CH, NH, OH, SH, CNH, COH, CSH, NOH, NSH, OSH, CNOH, CNSH, COSH, NOSH, CNOSH, CNOSPFCIBrIH}. Gradient boosting trees (GBTs) with the structured feature matrix are used for this computation.
A-B012-E-S-GBT	The barcodes same as those used in A-B012-E-C-GBT are used. Instead of <i>counts in bins</i> , the <i>Barcode statistics</i> method is used to generate features.
A-B012-E-SS-GBT	The barcodes same as those used in A-B012-E-C-GBT are used. The <i>persistence diagram slice and statistics</i> method is used to generate features. A uniform set of bins by dividing the interval [0,5] into 10 equal length bins is used to slice birth, death, and persistence values.
R-B012-E-S-GBT	Barcodes are generated using Rips complex with Euclidean distances. The features are generated following the <i>barcode statistics</i> method. Here 36 element combinations are considered, i.e., {C, N, O, S, CN, CO, CS, NO, NS, OS, CNO, CNS, COS, NOS, CNOS, CNOSPFCIBrI, H, CH, NH, OH, SH, CNH, COH, CSH, NOH, NSH, OSH, CNOH, CNSH, COSH, NOSH, CNOSH, CNOSPFCIBrIH, CCl, CClH, CBr, CBrH}.
R-B012-M1-S-GBT	The result is obtained with the same setup as R-B012-E-S-GBT except that the first level enrichment distance matrix \widetilde{M}^1 is used instead of Euclidean distance.
R-B _n -E-KNN	The Betti- <i>n</i> barcodes from Rips complex computation with Euclidean distance are used. K-nearest neighbor (KNN) regression is performed with Wasserstein metric d^2 . The leave-one-out validation is performed individually with each element combination and the average prediction of these element combinations is taken as the output result. The element combinations considered are {CNOS, CNOSPFCIBrI, NOH, CNO, CNOSPFCIBrIH}. These combinations are selected based on their performance in the gradient boosting trees experiments.
R-B _n -M1-KNN	The result is obtained with the same setup as R-B _n -E-KNN except that the distance matrix \widetilde{M}^n is used instead of Euclidean distance.

Table 1: Experiments for ligand-based protein-ligand binding affinity prediction of 7 protein clusters and 1322 protein-ligand complexes.

ID	Experiments	CL 1 (333)	CL 2 (264)	CL 3 (219)	CL 4 (156)	CL 5 (134)	CL 6 (122)	CL 7 (94)	Average
1	A-B012-E-C-GBT	0.695(1.63)	0.836(1.18)	0.690(1.52)	0.642(1.38)	0.840(1.30)	0.647(1.65)	0.730(1.27)	0.726(1.42)
2	A-B012-E-S-GBT	0.695(1.63)	0.845(1.14)	0.678(1.54)	0.692(1.31)	0.828(1.35)	0.702(1.54)	0.739(1.25)	0.740(1.39)
3	A-B012-E-SS-GBT	0.704(1.62)	0.846(1.15)	0.681(1.53)	0.668(1.35)	0.834(1.34)	0.715(1.53)	0.741(1.25)	0.741(1.40)
4	R-B012-E-S-GBT	0.712(1.60)	0.837(1.17)	0.659(1.57)	0.683(1.32)	0.808(1.41)	0.635(1.67)	0.757(1.22)	0.727(1.42)
5	R-B012-M1-S-GBT	0.716(1.59)	0.836(1.17)	0.706(1.48)	0.672(1.34)	0.822(1.37)	0.708(1.53)	0.746(1.24)	0.744(1.39)
6	2+5	0.714(1.59)	0.848(1.13)	0.699(1.50)	0.692(1.31)	0.831(1.34)	0.717(1.52)	0.747(1.24)	0.750(1.38)
7	R-B0-E-KNN	0.648(1.73)	0.761(1.39)	0.544(1.76)	0.616(1.42)	0.700(1.70)	0.487(1.89)	0.641(1.43)	0.628(1.62)
8	R-B1-E-KNN	0.547(1.91)	0.684(1.55)	0.444(1.88)	0.536(1.52)	0.535(2.01)	0.634(1.67)	0.649(1.42)	0.576(1.71)
9	R-B2-E-KNN	0.474(2.01)	0.494(1.87)	0.202(2.14)	0.298(1.79)	0.126(2.49)	0.331(2.09)	0.609(1.47)	0.362(1.98)
10	R-B0-M1-KNN	0.581(1.85)	0.771(1.35)	0.516(1.80)	0.601(1.44)	0.672(1.76)	0.485(1.90)	0.644(1.43)	0.610(1.65)
11	R-B1-M1-KNN	0.663(1.70)	0.784(1.33)	0.652(1.59)	0.555(1.50)	0.786(1.49)	0.610(1.71)	0.731(1.30)	0.683(1.52)
12	R-B2-M1-KNN	0.675(1.67)	0.803(1.28)	0.577(1.72)	0.531(1.52)	0.655(1.81)	0.617(1.72)	0.648(1.42)	0.644(1.59)
13	Cons(7+8+9+10+11+12)	0.698(1.66)	0.817(1.28)	0.620(1.68)	0.645(1.41)	0.756(1.68)	0.658(1.68)	0.739(1.31)	0.705(1.49)
14	2+5 (5-fold)	0.713(1.60)	0.843(1.15)	0.693(1.51)	0.670(1.35)	0.831(1.34)	0.698(1.56)	0.737(1.26)	0.741(1.40)
15	FFT-BP (5-fold) ¹¹²	(1.93)	(1.32)	(2.01)	(1.61)	(2.02)	(2.06)	(1.71)	(1.81)

Table 2: Pearson correlation coefficients with RMSE (kcal/mol) in parentheses for binding affinity predictions on 7 protein clusters (CL) in S1322. On the title row, the numbers in parentheses denote the numbers of ligands in the cluster. The median results of 20 repeated runs are reported for the ensemble of trees based methods to account for randomness in the algorithm. For experimental labels, the first letter indicates the complex definition used, 'A' for alpha complex and 'R' for Rips complex. The second part starting with 'B' followed by the integers indicates the Betti number used. The third part indicates the distance function used, 'E' for Euclidean and 'M1' for \widetilde{M}^1 . For row 1 through 5, the fourth part shows the way of feature construction, 'C' for counts in bins and 'S' for barcode statistics. The last part indicates the regression technique used, 'GBT' for gradient boosting trees and 'KNN' for k-nearest neighbors. The detailed descriptions of the experiments are given in Table 1. Row 6 is the results using features of both row 2 and row 5. Row 13 is the consensus results by taking the average of the predictions by row 7 through row 12. Except for specified, all results are obtained from 10-fold cross validations. FFT-BP 5-fold cross validation results were adopted from Ref.¹¹² where Pearson correlation coefficients were not given.

Robustness of topological models Certain elements such as Br are very rare in the data sets studied in this work. Considering only the elements of high occurrence will not hurt the performance on the validations performed. However, omitting the low occurrence elements will sacrifice the capability of the model to handle new data in which such elements play an important role. Therefore, we decide to keep the rare elements that result in a large number of features and redundancy in features. For example, the element combinations CBrH and CH will probably deliver the same performance for most of the samples in the data sets studied in this

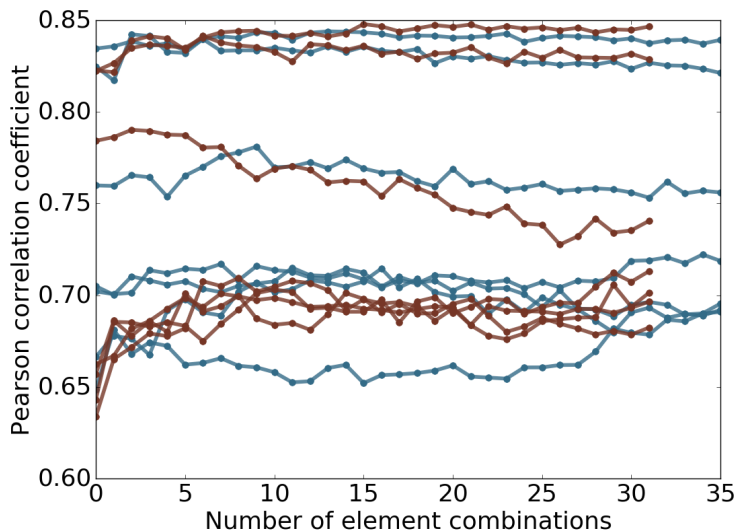


Figure 8: The model performance against the number of element combinations involved in feature construction for 7 protein clusters in S1322. The results related to alpha complex are marked in red and Rips complex in blue.

work. To test whether this redundancy causes degenerated results of the model, the features of one element combination is added to the model at a step and the model is validated with an accumulation of the added features at each step. The performance of the model is measured with Pearson correlation coefficient and is plotted against number of element combinations involved in Fig. 8. For most cases in Fig. 8, the model is robust against the inclusion of more element combinations.

III.B Complex based protein-ligand binding affinity prediction

Having demonstrated the representational power of the present topological method for characterizing small molecules, we further apply the proposed topological method to characterize both the protein and the ligand in a protein-ligand complex. Biologically, we consider the same task, i.e., the prediction of protein-ligand binding affinity, with a different approach that is based on the structural information of both the protein and the ligand in the protein-ligand complex. Only GBT and deep convolutional neural network algorithms are used in this section.

Version	Refined set	Training set	Core set (test set)	Protein families
v2007	1300	1105	195	65
v2013	2959	2764	195	65
v2015	3706	3511	195	65
v2016	4057	3767	290	58

Table 3: Number of complexes or number of protein families in PDBBind data sets used in the present binding affinity prediction. Here training sets are obtained from corresponding refined sets, excluding the complexes in corresponding test sets. Protein families refer to those in the corresponding tests.

Data sets The PDBBind database provides a comprehensive collection of structures of protein-ligand complexes and their binding affinity data.^{97,113} The original experimental data in Protein Data Bank (PDB)¹¹⁴ are selected to PDBBind database based on certain quality requirements and curated for applications. As shown in Table 3, this database is expanding on a yearly basis. It has become a standard resource for benchmarking computational methods and algorithms for protein-ligand binding analysis and drug design. Popular data sets include version 2007 (v2007), v2013, and v2015. Among them, v2013 core set and v2015 core set are identical. A large number of scoring functions has been tested on these data sets. The latest version, v2016, has an enlarged core set, which contains 290 protein-ligand complexes to represent 58 protein families. Therefore, this test set should be relatively easier than v2015 core set, whose 195 complexes involve 65 protein families.

In the present machine learning study, we use four PDBBind core sets as our test sets. For each test set, the corresponding refined set, excluding the core set, is used as the training set.

Groups of topological features and their performance in association with GBT The experiments of protein-ligand-complex-based protein-ligand binding affinity prediction for the PDBBind datasets are summarized in Table 4.

Experiment	Description
R-B0-I-C	Betti-0 barcodes from Rips complex computation with interactive distance matrix based on Euclidean distance are used. Features are generated following <i>counts in bins</i> method with bins $\{[0, 2.5), [2.5, 3), [3, 3.5), [3.5, 4.5), [4.5, 6), [6, 12]\}$. Element combinations used are all possible paired choices of one item from $\{C, N, O, S, CN, CO, NO, CNO\}$ in protein and another item from $\{C, N, O, S, P, F, Cl, Br, I, CN, CO, CS, NO, NS, OS, CNO, CNS, COS, NOS, CNOS\}$ in ligand, which result in a total of 160 combinations.
R-B0-I-BP	The persistent homology computation and feature generation is the same as R-B0-I-C. However, the element combinations used are all possible paired choices of one item from $\{C, N, O, S\}$ in protein and another item from $\{C, N, O, S, P, F, Cl, Br, I\}$ in ligand, which result in a total of 36 element combinations.
R-B0-CI-C	Betti-0 barcodes from Rips complex computation with interactive distance matrix based on the electrostatics correlation function defined in Eq. (8) with the parameter $c = 100$. The features are generated following <i>counts in bins</i> method with bins $\{(0, 0.1], (0.1, 0.2], (0.2, 0.3], (0.3, 0.4], (0.4, 0.5], (0.5, 0.6], (0.6, 0.7], (0.7, 0.8], (0.8, 0.9], (0.9, 1.0)\}$. The element combinations used are all possible paired choices of one item from $\{C, N, O, S, H\}$ in protein and another item from $\{C, N, O, S, P, F, Cl, Br, I, H\}$ in ligand, which result in a total of 50 element combinations.
R-B0-CI-B-S	The barcodes and element combinations are the same as those of R-B0-CI-B-C. The features are generated following the <i>barcode statistics</i> method.
A-B12-E-S	Betti-1 and Betti-2 barcodes from alpha complex computation with Euclidean distance are used. The element combinations considered are all heavy atoms and all carbon atoms. Features are generated following the <i>barcode statistics</i> method.

Table 4: Experiments for protein-ligand-complex-based protein-ligand binding affinity prediction for the PDBBind datasets.

ID	Experiments	v2007	v2013	v2015	v2016	Average
1	R-B0-I-C	0.799 (2.01)	0.741 (2.14)	0.750 (2.11)	0.813 (1.82)	0.776 (2.02)
2	R-B0-I-BP	0.816 (1.94)	0.741 (2.13)	0.750 (2.10)	0.825 (1.78)	0.783 (1.99)
3	R-B0-CI-C	0.791 (2.05)	0.759 (2.10)	0.738 (2.13)	0.801 (1.87)	0.772 (2.04)
4	R-B0-CI-S	0.773 (2.10)	0.762 (2.12)	0.749 (2.13)	0.810 (1.86)	0.774 (2.05)
5	A-B12-E-S	0.736 (2.25)	0.709 (2.26)	0.695 (2.27)	0.752 (2.02)	0.723 (2.20)
6	1+4	0.815 (1.95)	0.780 (2.04)	0.774 (2.04)	0.833 (1.76)	0.801 (1.95)
7	2+4	0.806 (1.99)	0.787 (2.04)	0.770 (2.06)	0.834 (1.77)	0.799 (1.97)
8	1+4+5	0.810 (1.98)	0.792 (2.02)	0.786 (2.02)	0.831 (1.76)	0.805 (1.95)
9	2+4+5	0.802 (2.01)	0.796 (2.02)	0.782 (2.04)	0.822 (1.79)	0.801 (1.97)
10	2D-CNN-Alpha	0.787 (2.02)	0.781 (1.98)	0.785 (1.95)	0.837 (1.68)	0.798 (1.91)
11	1D2D-CNN	0.806 (1.95)	0.781 (1.98)	0.799 (1.91)	0.848 (1.64)	0.809 (1.87)
12	RF::VinaElem ^a	0.803 (1.94) ¹¹⁵	0.752 (2.03) ¹¹⁶	-	-	-
13	RI-Score ^{101 b}	0.825^c (1.99)	-	0.782 ^d (2.05)	0.815 (1.85)	-

Table 5: Pearson correlation coefficients with RMSE (kcal/mol) in parentheses for predictions by various groups of features on the four PDBBind core sets. Results of ensemble of trees based methods (rows 1 through 9) are the *median values* of 50 repeated runs to account for randomness in the algorithm. For the deep learning based methods (row 10 and 11), 100 independent models are generated in the first place. A consensus model is built by randomly choosing 50 models out of the 100, and the this process is repeated 1000 times with the median reported. The first letter indicates the definition of complex, 'A' for alpha complex and 'R' for Rips complex. The second part indicates the Betti numbers used. The third part indicates the distance function used, 'I' for $\widehat{M}_{i,j}$ defined in 3, 'CI' for the one defined in 8, and 'E' for Euclidean. The last part shows the way of feature construction, 'C' for counts in bins, 'S' for barcode statistics, and 'BP' for only pair of two single elements. The results reported in row 6 through 9 are obtained by combining the features of the rows with the corresponding numbers. ^a The authors did not specify the number of repeated experiments and if the reported performance is the best or the median of the experiments. ^b The best results of the repeated runs with randomness are reported and the parameters in feature generation are optimized for each dataset. ^c The median PCC reported is 0.803. ^d The median PCC reported is 0.762.

Robustness of GBT algorithm against redundant element combination features and potential overfitting

It is intuitive that combinations of more than 2 element types are able to enrich the representation especially in the case of higher dimensional Betti numbers. However, the consideration of combination of more element types rapidly increases the dimensional of feature space. In the high dimensional feature space, it is almost inevitable that there exists nonessential and redundant features. Additionally, the importance of a feature varies across

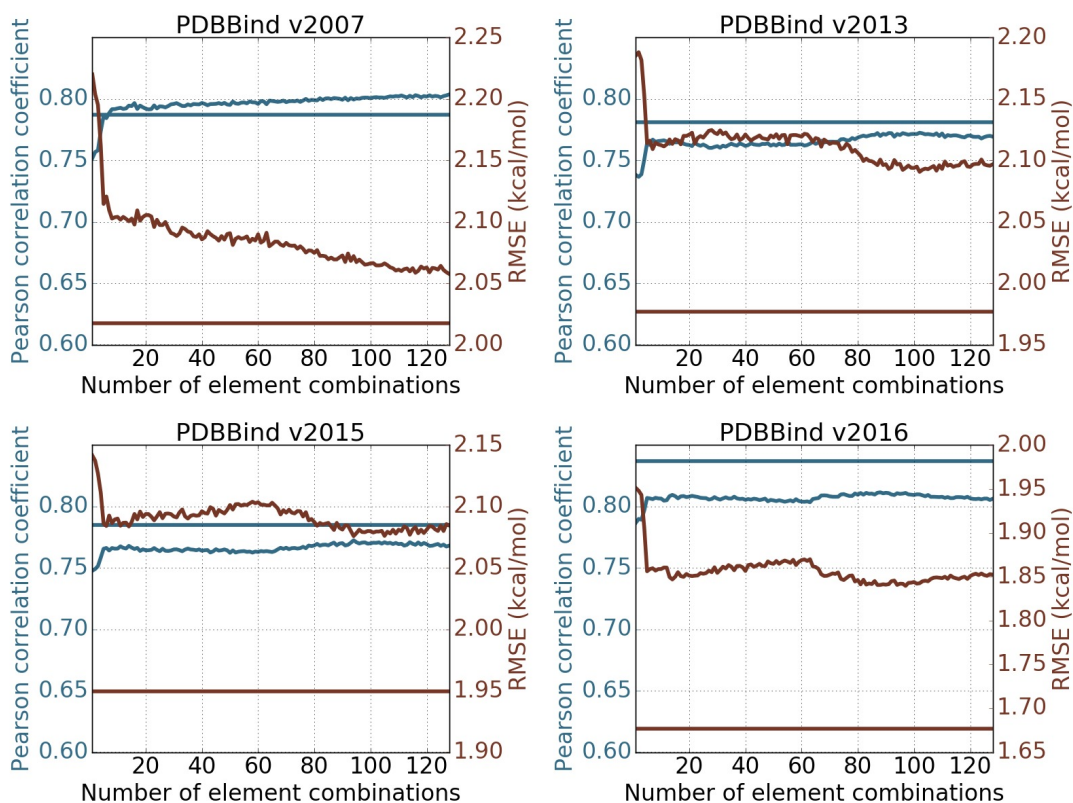


Figure 9: The performance of the model against the number of included element combinations. The Betti-1 and Betti-2 barcodes computed with alpha complex is used. Features are generated following *barcode statistics* method. Element combinations are all possible paired choices of one item from { C, N, O, CN, CO, NO, CNO, CNOS } in protein and another item from { C, N, O, S, CN, CO, CS, NO, NS, OS, CNO, CNS, COS, NOS, CNOS, CNOSPFCIBrI } in ligand, which result in 128 element combinations. The horizontal straight lines represents the performance of the 2D representation with deep convolutional neural network. The blue and red colors correspond to Pearson correlation coefficient and RMSE (kcal/mol) respectively.

different problems and data sets. Therefore, it is preferable to keep all the potentially important features in a general model which is expected to cover a wide range of situations. To test the robustness of the model against unimportant features, we select a total of 128 element combinations (i.e., all possible paired choices of one item from {C, N, O, CN, CO, NO, CNO, CNOS} in protein and another item from {C, N, O, S, CN, CO, CS, NO, NS, OS, CNO, CNS, COS, NOS, CNOS, CNOSPFCIBrI} in ligand). The Betti-0, Betti-1 and Betti-2 barcodes are computed for all combinations using alpha complex with Euclidean distance. Features are generated following the barcode statistics method.

A general model with all the features is generated in the first place. The element combinations are then sorted according to their importance scores in the general model. Starting from the most important element combination, one element combination is added to the feature vector each time and then the resulting feature vector is passed to the machine learning training and testing procedure. The level of adding element combinations is based on their importance scores and thus that a less important feature is added each step.

Figure 9 depicts the changes of Pearson correlation coefficient and RMSE (kcal/mol) with respect to the increase of element combinations in predicting four PDBBind core sets. In all cases, the inclusion of top combinations can readily deliver very good models. The behavior of the present method in PDBBind v2007 is quite different from that in other data sets. The performance of the present method improves almost monotonically as the element combination increases. However, in other three cases, the improvement is unsteady. Nevertheless, the performance fluctuates within a small range, which indicates that the present method is reasonably stable against the increase in element combinations. From a different perspective, the increase in element combinations might lead to overfitting in machine learning. Since the model parameters are fixed before the experiments, it shows that GBT algorithms are not very sensitive to redundant features and are robust against overfitting.

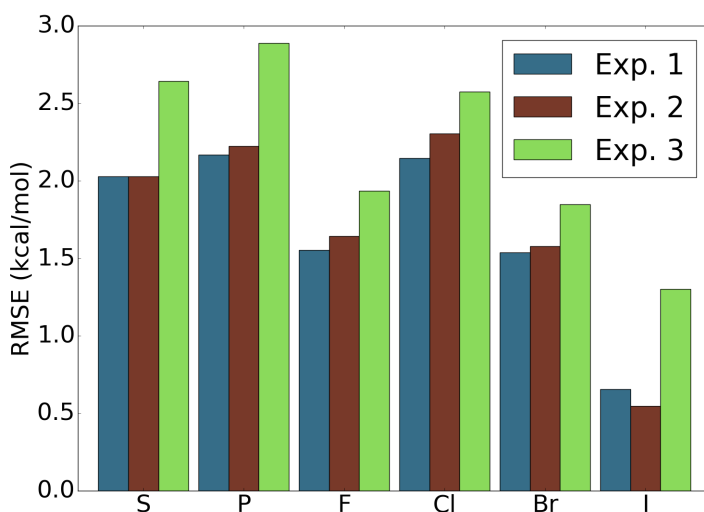


Figure 10: Assessment of performance of the model on samples with elements that are rare in the data sets. For the four data sets PDBBind v2007, v2013, v2015, and v2016,⁹⁷ and for each element, the testing set is the subset of the original core sets with only ligands that contain atoms of the particular element type. The features used are features with ID=7 in Table 5. The reported RMSE is the average taken over the four data sets. Experiment 1: Training set is the original training set and all the features are used. Experiment 2: Training set is the original training set and only features that do not involve the particular element are used. Experiment 3: Training set is the original training set excluding the samples that contain atoms of the particular element type and all features are used. For most of the elements, experiment 1 achieves the best result and experiment 3 yields the worst performance.

Usefulness of more than 2 element types for interactive Betti-0 barcodes While using element combinations with more than 2 element types with higher dimensional Betti numbers enriches characterization of geometry, it remains to assess whether interactive Betti-0 characterization will benefit from element combinations with more element types. As an example, we denote interactive Betti-0 barcodes for carbon and nitrogen atoms from protein and oxygen atoms from ligand by $\mathbf{B}_{\text{CN-O}}$, barcodes for carbon atoms from protein and oxygen atoms from ligand by $\mathbf{B}_{\text{C-O}}$, and barcodes for nitrogen atoms from protein and oxygen atoms from ligand by $\mathbf{B}_{\text{N-O}}$. In the case of persistent homology barcode representation, $\mathbf{B}_{\text{CN-O}}$ is not strictly the union of $\mathbf{B}_{\text{C-O}}$ and $\mathbf{B}_{\text{N-O}}$. However $\mathbf{B}_{\text{CN-O}}$ might be redundant to $\mathbf{B}_{\text{C-O}}$ and $\mathbf{B}_{\text{N-O}}$. To address this concern, we test features from interactive Betti-0 barcodes with the 36 element combinations (i.e., { C, N, O, S } for protein and { C, N, O, S, P, F, Cl, Br, I } for ligand) and features for the 160 selected element combinations (i.e., { C, N, O, S, CN, CO, NO, CNO } for protein and { C, N, O, S, P, F, Cl, Br, I, CN, CO, CS, NO, NS, OS, CNO, CNS, COS, NOS, CNOS } for ligand), which are listed as feature group 2 and feature group 1 in Table 5. In all the four cases, the features of the 36 combinations (feature group 2) slightly outperforms or performs as well as the features of the 160 combinations (feature group 1) suggesting that element combinations with more than 2 element types are redundant to all the combinations with 2 element types in the case of interactive Betti-0 characterization.

Importance of atomic charge information In element specific persistent homology, atoms of different element types are characterized separately, which offers a rough and implicit description of the electrostatics of the system. However, such implicit treatment of electrostatics may lose important information because atoms behave differently at different oxidation states. Therefore, we explicitly embed atomic charges in interactive Betti-0 barcodes as described in Eq. (8). The resulting topological features are given in feature group 4 in Table 5. It can be seen from Table 5 that the combination of feature group 4 and the Euclidean distance based interactive Betti-0 barcodes (listed as feature group 6 and 7) generally outperforms the results obtained with only Euclidean distance based features. This observation suggests that electrostatics play an important role and should be taken care of explicitly for the protein-ligand binding problem.

Relevance of elements that are rare with respect to the data sets Since the majority of the samples in both training and testing sets only contain atoms of element types, C, N, O, and H, the performance of the model on the samples with rare occurring elements with respect to data sets is hardly reflected by the overall performance statistics. For simplicity, we refer to such rarely occurring elements with respect to data sets simply

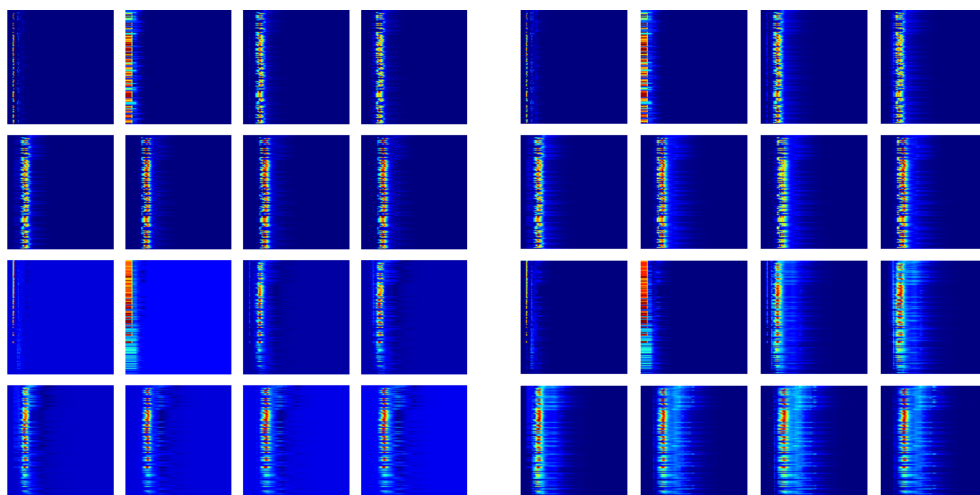


Figure 11: The heat map plot of the 16 channels. The mean value (left image) and the standard deviation (right image) of each digit over the PDBBind v2016 refined set are shown. The top 8 maps are for protein-ligand complex and the other 8 maps are for the difference between protein-ligand complex and protein only. For each map, the vertical axis is the element combinations ordered according to their importance and the horizontal axis is the dimension of spatial scales.

by rarely occurring elements in the discussion follows. To assess the aspects of the model that potentially affect the performance on the samples containing rarely occurring elements, we picked the samples containing each rarely occurring element from the original testing set as a new testing set. Three experiments are carried out to address two questions: “Are the training samples containing the same rarely occurring element crucial?” and “Are features addressing the rarely occurring element important?”. A short answer is yes to both according to the results shown in Figure 10. Specifically, for each rarely occurring element, the exclusion of samples containing this element in training set and the exclusion of features addressing this element will both cause degenerated results. It is also shown that the exclusion of samples of the rarely occurring element leads to much worse results. This observation suggests that the same interactions may lead to different binding properties for molecules with different compositions. Since both modifications of the model deliver worse results, we conclude that including the samples in the training set with similar compositions to the test sample is crucial to the success of the model on this specific test sample. Even the inclusion of features of more element types or element combinations does not deliver better results in the general testing sets, such features should still be kept in the model in case that a sample with a similar element composition comes in as a test sample.

2D persistence for deep convolutional neural networks Deep learning is potentially more powerful than many other machine learning algorithms when the data size is sufficiently large. In the present work, it is natural to construct a 2D representation by incorporating the element combination as an additional dimension, resulting in 16 channels as defined in Section II.E. Here 128 element combinations (i.e., all possible paired choices of one item from {C, N, O, CN, CO, NO, CNO, CNOS} in protein and another item from {C, N, O, S, CN, CO, CS, NO, NS, OS, CNO, CNS, COS, NOS, CNOS, CNOSPFClBrI} in ligand) are used for 2D analysis. The advantage of introducing this extra dimension with convolutional neural networks is to prevent unimportant features from interacting with important ones at the lower levels of the model whilst generally unimportant features are still kept in the model in case that they are essential to specific problems or a certain portion of the data set. Figure 11 illustrates the mean value and the standard deviation of the PDBBind v2016 refined set. The existence of significant standard deviations for relatively unimportant element combinations indicates that these features might still contribute to the overall prediction.

As shown in Figure 9, for all the data sets except the PDBBind v2007 set, the 2D representation with convolutional neural networks performs significantly better. The inferior performance of convolutional neural networks in v2007 might be a result of the small data size. Note that v2017 training set has 1102 protein-ligand complexes, whereas other training sets have more than 2700 complexes. Consequently, deep convolutional neural networks are able to outperform the GBT algorithm in predicting v2013, v2015 and v2016 core sets. Indeed, deep convolutional neural networks have advantages in dealing with large data sets.

III.C Structure-based virtual screening

In this section, we examine the performance of the proposed method for the main application in this paper, which is structure-based virtual screening. The dataset is much larger than the two applications on protein-ligand binding affinity prediction. Therefore, the best performing procedures in ligand-based binding affinity prediction and protein-ligand-complex-based binding affinity prediction are applied in this virtual screening application, since tuning parameters on such big dataset is too time consuming.

DUD data set The directory of useful decoys (DUD)^{117,118} is used to benchmark our topological approach for virtual screening. The DUD data set contains 40 protein targets from six classes, i.e., nuclear hormone receptors, kinases, serine proteases, metalloenzymes, folate enzymes, and other enzymes. A total of about 3000 active ligands were identified from literature. The number of ligands for each target ranges from tens to hundreds. At most 36 decoys were constructed for each ligand, from the ZINC database of commercially available compounds.¹¹⁹ The decoys were selected so that they possess similar physical properties to the ligands but have dissimilar molecular topology. The physical properties include molecular weight, the log P value, and number of hydrogen bonding groups. This results in a total of about 100000 compounds. A discrepancy between calculated partial charges for the ligand and decoy sets was reported for the original release 2 of DUD datasets, which makes it trivial for virtual screening methods to distinguish between the two sets using those charges. In this work, we use the sets with recalculated Gasteiger charges for both ligand and decoy sets.¹²⁰

Data processing In structure-based virtual screening, the possible complex structures of the target protein and the small molecule candidate are required. For the DUD dataset, the structures of the 40 protein targets, the ligands, and the decoys are given, and we generate protein-ligand complexes or protein-decoy complexes by using docking software. To this end, we first add missing atoms to proteins by using the profix utility in Jackal software package.¹²¹ The receptors and ligands or decoys are prepared using the scripts `prepare_receptor4.py` and `prepare_ligand4.py` provided by the AutoDockTools module in MGLTools package (version 1.5.6).¹²² The bounding box of the binding site is defined as a cube with edge size equal to 27 Å, centered at the geometric center of the crystal ligand. AutoDock Vina (version 1.1.2)¹²³ is used to dock the ligand or decoy to the receptor. The option `exhaustiveness` is set to 16 and all the other parameters are set to their default values. In each docking experiment, the pose having the lowest binding free energy reported by AutoDock Vina, is used by the machine learning based model.

Method	Parameters
GBT	n=2000, s=0.5, cw=100:1, lr=0.01, mf=sqrt
RF	n=2000, cw=balanced_subsample
ET	n=2000, cw=balanced_subsample

Table 6: The parameters used for the ensemble of trees methods while the other parameters are set to default. GBT: gradient boosting trees. RF: random forest. ET: extra trees. n: n_estimators. s: subsample. cw: class_weight. lr: learning_rate. mf: max_feature

Evaluation Two metrics, the enrichment factor (EF) and the area under the receiver operating characteristic curve (AUC), are used to evaluate each method’s ability of discriminating ligands from decoys. The AUC is defined as

$$\text{AUC} = 1 - \frac{1}{N_a} \sum_{i=1}^{N_a} \frac{N_d^i}{N_d}, \quad (14)$$

where N_a is the number of active ligands, N_d is the total number of decoys, and N_d^i is the number of decoys that are higher ranked than the i th ligand. An AUC value of 0.5 is the expected value of random selection, whereas a perfect prediction results in an AUC of 1. The EF at $x\%$ denoted by $\text{EF}_{x\%}$ evaluates the quality of the set of top $x\%$ ranked compounds, by comparing the percentage of actives in the top $x\%$ ranked compounds to the percentage of actives in the entire compound set. It is defined as

$$\text{EF}_{x\%} = \frac{N_a^{x\%}}{N^{x\%}} \cdot \frac{N}{N_a}, \quad (15)$$

where $N_a^{x\%}$ is the number of active ligands in the top $x\%$ ranked compounds, $N^{x\%}$ is the number of top $x\%$ ranked compounds, N is the total number of compounds, and N_a is the total number of active ligands.

Target	ADV			TopVS-ML		
	EF _{2%}	EF _{20%}	AUC	EF _{2%}	EF _{20%}	AUC
ACE	4.1	1.4	0.42	5.1	3.2	0.81
AChE	4.7	2.8	0.67	0.5	1.2	0.61
ADA	0.0	0.4	0.49	13.0	3.7	0.89
ALR2	2.0	2.7	0.74	2.0	1.4	0.67
AmpC	2.4	0.2	0.34	0.0	0.2	0.53
AR	17.0	3.8	0.81	19.5	4.3	0.90
CDK2	9.0	2.4	0.64	3.8	3.8	0.85
COMT	13.1	1.4	0.56	17.4	2.7	0.74
COX1	9.9	2.8	0.76	9.9	3.2	0.84
COX2	20.7	3.9	0.86	18.7	4.9	0.97
DHFR	6.4	2.8	0.82	13.0	4.7	0.96
EGFr	3.4	1.6	0.63	19.5	4.8	0.96
ER _{agonist}	17.8	3.3	0.84	9.3	3.0	0.81
ER _{antagonist}	10.2	2.3	0.70	0.0	3.6	0.86
FGFr1	0.4	0.8	0.44	10.9	4.8	0.95
FXa	1.0	1.3	0.63	1.7	4.3	0.89
GART	0.0	1.9	0.75	2.6	0.6	0.49
GPB	0.0	0.9	0.48	0.0	2.2	0.71
GR	5.7	1.2	0.57	0.0	2.6	0.77
HIVPR	5.6	2.6	0.74	4.8	4.2	0.90
HIVRT	8.2	1.9	0.64	9.4	4.1	0.88
HMGR	0.0	0.9	0.53	23.1	5.0	0.98
HSP90	0.0	0.9	0.64	5.5	4.5	0.93
InhA	13.4	1.9	0.56	22.7	4.5	0.95
MR	16.7	4.0	0.82	6.7	4.7	0.89
NA	0.0	0.3	0.37	1.0	3.5	0.84
P38 MAP	1.4	1.7	0.59	17.7	4.5	0.95
PARP	4.2	2.7	0.71	0.0	2.4	0.74
PDE5	8.0	1.9	0.61	6.9	3.5	0.86
PDGFr _b	3.5	0.5	0.32	20.3	4.9	0.96
PNP	0.0	0.7	0.59	8.9	4.1	0.90
PPAR _g	17.7	3.4	0.82	0.6	1.6	0.72
PR	1.9	1.1	0.52	9.4	4.0	0.88
RXR _a	28.2	4.8	0.95	7.7	2.5	0.79
SAHH	10.4	3.0	0.80	1.5	4.2	0.84
SRC	5.6	2.3	0.71	20.2	4.9	0.97
thrombin	8.3	2.6	0.72	2.8	2.2	0.75
TK	0.0	0.9	0.56	6.9	2.5	0.64
trypsin	3.1	1.9	0.58	0.0	2.0	0.74
VEGFr ₂	10.2	2.2	0.63	21.0	4.7	0.96
Average	6.9	2.0	0.64	8.6	3.4	0.83

Table 7: The median results of 10 repeated runs with different random seeds are reported. The best AUC in each row is marked in bold. The second block of AutoDock Vina (ADV) results are acquired from our ADV runs. The number of ligands for each target is listed in the parenthesis next the target name.

Topology based machine learning models Unlike physical based models, a training set of sufficient size is needed for machine learning based models. To evaluate the performance of various methods on the DUD data set, the structure data obtained from docking associated with one protein target are used as the test set each time.¹⁰⁹ For the selection of the training set of a given protein target, we follow a procedure given in the literature,¹¹⁷ where the entries associated to the rest of the proteins, excluding those that are within the same class of the testing protein and those that have reported positive cross-enrichment with the testing protein, are

taken as the training set. The 40 proteins are split into 6 classes.¹¹¹ A detailed list of proteins that are excluded from the training set of each protein is given in Supplementary Table S6.

Method	AUC	Ref
TopVS-ML	0.83	
DeepVS-ADV	0.81	109
ICM ^a	0.79	124
NNScore1-ADV ^b	0.78	110
Glide SP ^a	0.77	125
DDFA-ALL	0.77	111
DDFA-RL	0.76	111
NNScore2-ADV ^b	0.76	110
DDFA-ADV	0.75	111
DeepVS-Dock	0.74	109
DDFA-AD4	0.74	111
Glide HTVS ^b	0.73	110
Surflex ^a	0.72	125
Glide HTVS	0.72	125
ICM	0.71	124
RAW-ALL	0.70	111
AutoDock Vina ^b	0.70	110
Surflex	0.66	125
Rosetta Ligand	0.65	111
AutoDock Vina	0.64	111
ICM	0.63	125
FlexX	0.61	125
Autodock4.2	0.60	111
PhDOCK	0.59	125
Dock4.0	0.55	125

Table 8: ^aTuned by expert knowledge. ^bDetermined using a different data set of decoys.

Our topology based machine learning model, called *TopVS-ML*, relies on manually constructed features and utilizes ensemble of trees methods. For the complex with the small molecules (i.e., ligands and decoys) docked to the receptor, features R-B0-I-BP, R-B0-CI-S, and A-B12-E-S are used, whereas features R-B012-M1-S and A-B012-E-S are used for the small molecules. The gradient boosting trees method, random forest method, and extra trees method are employed as voters. The averaged probabilities output by the three methods are used for the classifier to decide the class of the testing samples. The modules *GradientBoostingClassifier*, *RandomForestClassifier*, and *ExtraTreesClassifier* in the scikit-learn package¹⁰⁶ are used. The parameters for the three modules are listed in Table 6. The performance on each of 40 protein targets is reported in Table 7. We have also generated virtual screening results of AutoDock Vina (ADV) based on the modeled binding free energy and compared them with those of the present TopVS-ML in terms of enrichment factors and the areas under the receiver operating characteristic curve (AUC). A comprehensive comparison of average AUC with those from a large number of methods is given in Table 8.

In our final model reported in Table 8, we use topological descriptors of both protein-compound interactions and only the compounds (i.e., ligands and decoys). We have also tested our models using either one of the aforementioned descriptions. When only topological descriptor of small molecules are used, which falls into the category of ligand-based virtual screening, an AUC of 0.81 is achieved. For the topological model using only the descriptions of protein-ligand interactions, an AUC of 0.77 are achieved. An AUC of 0.83 is obtained with a model combining both sets of descriptors which is better than each individual performance, suggesting that the two groups of descriptors are complementary to each other and are both important for achieving satisfactory results. The marginal improvement made by protein-compound complexes maybe due to the various docking quality. Similar situation was encountered by a deep learning method.¹⁰⁹ For the targets with high quality results by AutoDock Vina (AUC of ADV > 0.8), the ligand-based features achieve an AUC of 0.81 and the complex-based

features achieve an AUC of 0.86. On the other hand, for the targets with low quality results by Autodock Vina (AUC of ADV < 0.5), the ligand-based features achieve an AUC of 0.81 and the complex-based features achieve an AUC of 0.74. The results of these cases are listed in Table S8 and S9. This observation suggests that the performance of features describing the interactions and the geometry of protein-compounds complexes highly depends on the quality of docking results.

Our model with small molecular descriptors delivers an AUC of 0.81, which is comparably well to the other top performing methods. The performance of this model is also competitive in the regime of protein-ligand binding affinity prediction based on experimentally solved complex structures as is shown in Section III.A. These results suggest that topology based small molecule characterization proposed in this work is potentially useful in other applications to small molecules, such as predictions of toxicity, solubility and partition coefficient.

IV Conclusion

Persistent homology is a relatively new branch of algebraic topology and is the main workhorse in topological data analysis. The topological simplification of biomolecular systems was a major motivation of the earlier persistent homology development.^{29,36} Persistent homology has been applied to computational biology,^{76,77,77-79} including our efforts.^{26,87-91,93} However, the predictive power of primitive persistent homology was limited in early applications.⁹² To address this challenge, we have recently introduced element specific persistent homology to retain chemical and biological information during the topological abstraction of biomolecules.^{14,27,94} This approach offers competitive predictions of protein-ligand binding affinity and mutation induced protein stability changes. However, its representability and predictive power for small molecules and their interaction with macromolecules remain unknown.

The present work further introduces multicomponent persistent homology, multi-level persistent homology and electrostatic persistence for chemical and biological characterization, analysis and modeling. Multicomponent persistent homology takes a combinatorial approach to create possible element specific topological representations. Multi-level persistent homology allows tailored topological descriptions of any desirable interaction in biomolecules. Electrostatic persistence incorporates partial charges that are essential to biomolecules in topological invariants. These approaches are implemented via the appropriate construction of the distance matrix for filtration. The representation power and reduction power of multicomponent persistent homology, multi-level persistent homology and electrostatic persistence are validated by two databases, namely PDBBind⁹⁷ and DUD.^{117,118} PDBBind involves more than 4,000 protein-ligand complexes and DUD contains near 100,000 small compounds. Two classes of problems are used to test the proposed topological methods, including the regression (prediction) of protein-ligand binding affinities and the discrimination of active ligands from non-active decoys (virtual screening). In both problems, we examine the representability of proposed topological methods on small molecules, which are somewhat more difficult to describe by persistent homology due to their chemical diversity, variability and sensitivity. Additionally, these methods are tested on their ability to handle the full protein-ligand complexes. Advanced machine learning methods, including Wasserstein metric based k nearest neighbors (KNNs), gradient boosting trees (GBTs), random forest (RF), extra trees (ETs) and deep convolutional neural networks (CNNs) are utilized in the present work to facilitate the proposed topological methods in quantitative biomolecular predictions. The thorough examination of the method on the prediction of binding affinity for experimentally solved protein-ligand complexes leads to a structure-based virtual screening method, TopVS, which outperforms other modern methods. The feature sets introduced in this work for small molecules and protein-ligand complexes can be extended to other applications such as 3D-structure based prediction of toxicity, solubility, and partition coefficient for small molecules and complex structure based prediction of protein-nucleic acid binding and protein-protein binding affinities.

Acknowledgment

This work was supported in part by NSF Grants DMS-1721024 and IIS-1302285 and MSU Center for Mathematical Molecular Biosciences Initiative.

References

- [1] A. Krizhevsky, I. Sutskever, and G. E. Hinton, "Imagenet classification with deep convolutional neural networks," in *Advances in neural information processing systems*, pp. 1097-1105, 2012.

- [2] K. Simonyan and A. Zisserman, "Very deep convolutional networks for large-scale image recognition," *arXiv preprint arXiv:1409.1556*, 2014.
- [3] Y. LeCun, Y. Bengio, and G. Hinton, "Deep learning," *Nature*, vol. 521, no. 7553, pp. 436–444, 2015.
- [4] G. Hinton, L. Deng, D. Yu, G. E. Dahl, A.-r. Mohamed, N. Jaitly, A. Senior, V. Vanhoucke, P. Nguyen, T. N. Sainath, and B. Kingsbury, "Deep neural networks for acoustic modeling in speech recognition: The shared views of four research groups," *IEEE Signal Processing Magazine*, vol. 29, no. 6, pp. 82–97, 2012.
- [5] J. Schmidhuber, "Deep learning in neural networks: An overview," *Neural Networks*, vol. 61, pp. 85–117, 2015.
- [6] J. Ngiam, A. Khosla, M. Kim, J. Nam, H. Lee, and A. Y. Ng, "Multimodal deep learning," in *Proceedings of the 28th international conference on machine learning (ICML-11)*, pp. 689–696, 2011.
- [7] T. B. Hughes, G. P. Miller, and S. J. Swamidass, "Modeling epoxidation of drug-like molecules with a deep machine learning network," 2015.
- [8] T. Unterthiner, A. Mayr, G. Klambauer, and S. Hochreiter, "Toxicity prediction using deep learning," *arXiv preprint arXiv:1503.01445*, 2015.
- [9] A. Lusci, G. Pollastri, and P. Baldi, "Deep architectures and deep learning in chemoinformatics: the prediction of aqueous solubility for drug-like molecules," *Journal of chemical information and modeling*, vol. 53, no. 7, pp. 1563–1575, 2013.
- [10] I. Wallach, M. Dzamba, and A. Heifets, "Atomnet: A deep convolutional neural network for bioactivity prediction in structure-based drug discovery," *arXiv preprint arXiv:1510.02855*, 2015.
- [11] G. E. Dahl, N. Jaitly, and R. Salakhutdinov, "Multi-task neural networks for qsar predictions," *arXiv preprint arXiv:1406.1231*, 2014.
- [12] B. Ramsundar, S. Kearnes, P. Riley, D. Webster, D. Konerding, and V. Pande, "Massively multitask networks for drug discovery," *arXiv preprint arXiv:1502.02072*, 2015.
- [13] Z. Wu, B. Ramsundar, E. N. Feinberg, J. Gomes, C. Geniesse, A. S. Pappu, K. Leswing, and V. Pande, "Moleculenet: A benchmark for molecular machine learning," *arXiv preprint arXiv:1703.00564*, 2017.
- [14] Z. X. Cang and G. W. Wei, "Analysis and prediction of protein folding energy changes upon mutation by element specific persistent homology," *Bioinformatics*, in press, 2017.
- [15] P. W. Bates, G. W. Wei, and S. Zhao, "Minimal molecular surfaces and their applications," *Journal of Computational Chemistry*, vol. 29, no. 3, pp. 380–91, 2008.
- [16] P. W. Bates, Z. Chen, Y. H. Sun, G. W. Wei, and S. Zhao, "Geometric and potential driving formation and evolution of biomolecular surfaces," *J. Math. Biol.*, vol. 59, pp. 193–231, 2009.
- [17] Q. Zheng, S. Y. Yang, and G. W. Wei, "Molecular surface generation using PDE transform," *International Journal for Numerical Methods in Biomedical Engineering*, vol. 28, pp. 291–316, 2012.
- [18] Z. Chen, N. A. Baker, and G. W. Wei, "Differential geometry based solvation models I: Eulerian formulation," *J. Comput. Phys.*, vol. 229, pp. 8231–8258, 2010.
- [19] Z. Chen, N. A. Baker, and G. W. Wei, "Differential geometry based solvation models II: Lagrangian formulation," *J. Math. Biol.*, vol. 63, pp. 1139–1200, 2011.
- [20] Z. Chen, S. Zhao, J. Chun, D. G. Thomas, N. A. Baker, P. B. Bates, and G. W. Wei, "Variational approach for nonpolar solvation analysis," *Journal of Chemical Physics*, vol. 137, no. 084101, 2012.
- [21] D. D. Nguyen and G. W. Wei, "The impact of surface area, volume, curvature and lennard-jones potential to solvation modeling," *Journal of Computational Chemistry*, vol. 38, pp. 24–36, 2017.

- [22] X. Feng, K. Xia, Y. Tong, and G.-W. Wei, "Geometric modeling of subcellular structures, organelles and large multiprotein complexes," *International Journal for Numerical Methods in Biomedical Engineering*, vol. 28, pp. 1198–1223, 2012.
- [23] X. Feng, K. L. Xia, Y. Y. Tong, and G. W. Wei, "Multiscale geometric modeling of macromolecules II: lagrangian representation," *Journal of Computational Chemistry*, vol. 34, pp. 2100–2120, 2013.
- [24] K. L. Xia, X. Feng, Y. Y. Tong, and G. W. Wei, "Multiscale geometric modeling of macromolecules I: Cartesian representation," *Journal of Computational Physics*, vol. 275, pp. 912–936, 2014.
- [25] S. M. Kandathil, T. L. Fletcher, Y. Yuan, J. Knowles, and P. L. Popelier, "Accuracy and tractability of a kriging model of intramolecular polarizable multipolar electrostatics and its application to histidine," *Journal of computational chemistry*, vol. 34, no. 21, pp. 1850–1861, 2013.
- [26] K. L. Xia and G. W. Wei, "Persistent homology analysis of protein structure, flexibility and folding," *International Journal for Numerical Methods in Biomedical Engineerings*, vol. 30, pp. 814–844, 2014.
- [27] Z. X. Cang and G. W. Wei, "Integration of element specific persistent homology and machine learning for protein-ligand binding affinity prediction," *International Journal for Numerical Methods in Biomedical Engineering*, Accepted, 2017.
- [28] T. Schlick and W. K. Olson, "Trefoil knotting revealed by molecular dynamics simulations of supercoiled DNA," *Science*, vol. 257, no. 5073, pp. 1110–1115, 1992.
- [29] A. Zomorodian and G. Carlsson, "Computing persistent homology," *Discrete Comput. Geom.*, vol. 33, pp. 249–274, 2005.
- [30] D. W. Sumners, "Knot theory and DNA," in *Proceedings of Symposia in Applied Mathematics*, vol. 45, pp. 39–72, 1992.
- [31] I. K. Darcy and M. Vazquez, "Determining the topology of stable protein-DNA complexes," *Biochemical Society Transactions*, vol. 41, pp. 601–605, 2013.
- [32] C. Heitsch and S. Poznanovic, "Combinatorial insights into rna secondary structure, in N. Jonoska and M. Saito, editors," *Discrete and Topological Models in Molecular Biology*, vol. Chapter 7, pp. 145–166, 2014.
- [33] O. N. A. Demerdash, M. D. Daily, and J. C. Mitchell, "Structure-based predictive models for allosteric hot spots," *PLOS Computational Biology*, vol. 5, p. e1000531, 2009.
- [34] B. DasGupta and J. Liang, *Models and Algorithms for Biomolecules and Molecular Networks*. John Wiley & Sons, 2016.
- [35] X. Shi and P. Koehl, "Geometry and topology for modeling biomolecular surfaces," *Far East J. Applied Math.*, vol. 50, pp. 1–34, 2011.
- [36] H. Edelsbrunner, D. Letscher, and A. Zomorodian, "Topological persistence and simplification," *Discrete Comput. Geom.*, vol. 28, pp. 511–533, 2002.
- [37] P. Bendich and J. Harer, "Persistent intersection homology," *Foundations of Computational Mathematics (FOCM)*, vol. 11, no. 3, pp. 305–336, 2011.
- [38] D. Cohen-Steiner, H. Edelsbrunner, and J. Harer, "Stability of persistence diagrams," *Discrete & Computational Geometry*, vol. 37, no. 1, pp. 103–120, 2007.
- [39] D. Cohen-Steiner, H. Edelsbrunner, and J. Harer, "Extending persistence using poincaré and lefschetz duality," *Foundations of Computational Mathematics*, vol. 9, no. 1, pp. 79–103, 2009.
- [40] D. Cohen-Steiner, H. Edelsbrunner, J. Harer, and D. Morozov, "Persistent homology for kernels, images, and cokernels," in *Proceedings of the Twentieth Annual ACM-SIAM Symposium on Discrete Algorithms, SODA 09*, pp. 1011–1020, 2009.

- [41] F. Chazal, D. Cohen-Steiner, M. Glisse, L. J. Guibas, and S. Oudot, "Proximity of persistence modules and their diagrams," in *Proc. 25th ACM Sympos. on Comput. Geom.*, pp. 237–246, 2009.
- [42] F. Chazal, L. J. Guibas, S. Y. Oudot, and P. Skraba, "Persistence-based clustering in riemannian manifolds," in *Proceedings of the 27th annual ACM symposium on Computational geometry*, SoCG '11, pp. 97–106, 2011.
- [43] G. Carlsson and A. Zomorodian, "The theory of multidimensional persistence," *Discrete Computational Geometry*, vol. 42, no. 1, pp. 71–93, 2009.
- [44] G. Carlsson, V. de Silva, and D. Morozov, "Zigzag persistent homology and real-valued functions," in *Proc. 25th Annu. ACM Sympos. Comput. Geom.*, pp. 247–256, 2009.
- [45] V. de Silva, D. Morozov, and M. Vejdemo-Johansson, "Persistent cohomology and circular coordinates," *Discrete and Comput. Geom.*, vol. 45, pp. 737–759, 2011.
- [46] G. Carlsson and V. De Silva, "Zigzag persistence," *Foundations of computational mathematics*, vol. 10, no. 4, pp. 367–405, 2010.
- [47] S. Y. Oudot and D. R. Sheehy, "Zigzag Zoology: Rips Zigzags for Homology Inference," in *Proc. 29th Annual Symposium on Computational Geometry*, pp. 387–396, June 2013.
- [48] T. K. Dey, F. Fan, and Y. Wang, "Computing topological persistence for simplicial maps," in *Proc. 30th Annu. Sympos. Comput. Geom. (SoCG)*, pp. 345–354, 2014.
- [49] K. Mischaikow and V. Nanda, "Morse theory for filtrations and efficient computation of persistent homology," *Discrete and Computational Geometry*, vol. 50, no. 2, pp. 330–353, 2013.
- [50] A. Tausz, M. Vejdemo-Johansson, and H. Adams, "Javaplex: A research software package for persistent (co)homology." Software available at <http://code.google.com/p/javaplex>, 2011.
- [51] V. Nanda, "Perseus: the persistent homology software." Software available at <http://www.sas.upenn.edu/~vnanda/perseus>.
- [52] U. Bauer, M. Kerber, and J. Reininghaus, "Distributed computation of persistent homology," *Proceedings of the Sixteenth Workshop on Algorithm Engineering and Experiments (ALENEX)*, 2014.
- [53] G. Carlsson, A. Zomorodian, A. Collins, and L. J. Guibas, "Persistence barcodes for shapes," *International Journal of Shape Modeling*, vol. 11, no. 2, pp. 149–187, 2005.
- [54] R. Ghrist, "Barcodes: The persistent topology of data," *Bull. Amer. Math. Soc.*, vol. 45, pp. 61–75, 2008.
- [55] H. Edelsbrunner and J. Harer, *Computational topology: an introduction*. American Mathematical Soc., 2010.
- [56] G. Carlsson, G. Singh, and A. Zomorodian, "Computing multidimensional persistence," in *Algorithms and computation*, pp. 730–739, Springer, 2009.
- [57] G. Carlsson, T. Ishkhanov, V. Silva, and A. Zomorodian, "On the local behavior of spaces of natural images," *International Journal of Computer Vision*, vol. 76, no. 1, pp. 1–12, 2008.
- [58] D. Pachauri, C. Hinrichs, M. Chung, S. Johnson, and V. Singh, "Topology-based kernels with application to inference problems in alzheimer's disease," *Medical Imaging, IEEE Transactions on*, vol. 30, pp. 1760–1770, Oct 2011.
- [59] G. Singh, F. Memoli, T. Ishkhanov, G. Sapiro, G. Carlsson, and D. L. Ringach, "Topological analysis of population activity in visual cortex," *Journal of Vision*, vol. 8, no. 8, 2008.
- [60] P. Bendich, H. Edelsbrunner, and M. Kerber, "Computing robustness and persistence for images," *IEEE Transactions on Visualization and Computer Graphics*, vol. 16, pp. 1251–1260, 2010.

- [61] P. Frosini and C. Landi, “Persistent betti numbers for a noise tolerant shape-based approach to image retrieval,” *Pattern Recognition Letters*, vol. 34, pp. 863–872, 2013.
- [62] J. A. Perea and J. Harer, “Sliding windows and persistence: An application of topological methods to signal analysis,” *Foundations of Computational Mathematics*, vol. 15, pp. 799–838, 2015.
- [63] K. Mischaikow, M. Mrozek, J. Reiss, and A. Szymczak, “Construction of symbolic dynamics from experimental time series,” *Physical Review Letters*, vol. 82, pp. 1144–1147, 1999.
- [64] T. Kaczynski, K. Mischaikow, and M. Mrozek, *Computational Homology*, vol. 157 of *Applied Mathematical Sciences*. New York: Springer-Verlag, 2004.
- [65] V. D. Silva and R. Ghrist, “Blind swarms for coverage in 2-d,” in *In Proceedings of Robotics: Science and Systems*, p. 01, 2005.
- [66] H. Lee, H. Kang, M. K. Chung, B. Kim, and D. S. Lee, “Persistent brain network homology from the perspective of dendrogram,” *Medical Imaging, IEEE Transactions on*, vol. 31, pp. 2267–2277, Dec 2012.
- [67] D. Horak, S. Maletic, and M. Rajkovic, “Persistent homology of complex networks,” *Journal of Statistical Mechanics: Theory and Experiment*, vol. 2009, no. 03, p. P03034, 2009.
- [68] G. Carlsson, “Topology and data,” *Am. Math. Soc*, vol. 46, no. 2, pp. 255–308, 2009.
- [69] P. Niyogi, S. Smale, and S. Weinberger, “A topological view of unsupervised learning from noisy data,” *SIAM Journal on Computing*, vol. 40, pp. 646–663, 2011.
- [70] B. Wang, B. Summa, V. Pascucci, and M. Vejdemo-Johansson, “Branching and circular features in high dimensional data,” *IEEE Transactions on Visualization and Computer Graphics*, vol. 17, pp. 1902–1911, 2011.
- [71] B. Rieck, H. Mara, and H. Leitte, “Multivariate data analysis using persistence-based filtering and topological signatures,” *IEEE Transactions on Visualization and Computer Graphics*, vol. 18, pp. 2382–2391, 2012.
- [72] X. Liu, Z. Xie, and D. Yi, “A fast algorithm for constructing topological structure in large data,” *Homology, Homotopy and Applications*, vol. 14, pp. 221–238, 2012.
- [73] B. Di Fabio and C. Landi, “A mayer-vietoris formula for persistent homology with an application to shape recognition in the presence of occlusions,” *Foundations of Computational Mathematics*, vol. 11, pp. 499–527, 2011.
- [74] P. K. Agarwal, H. Edelsbrunner, J. Harer, and Y. Wang, “Extreme elevation on a 2-manifold,” *Discrete and Computational Geometry (DCG)*, vol. 36, no. 4, pp. 553–572, 2006.
- [75] X. Feng and Y. Tong, “Choking loops on surfaces,” *IEEE Transactions on Visualization and Computer Graphics*, vol. 19, no. 8, pp. 1298–1306, 2013.
- [76] P. M. Kasson, A. Zomorodian, S. Park, N. Singhal, L. J. Guibas, and V. S. Pande, “Persistent voids a new structural metric for membrane fusion,” *Bioinformatics*, vol. 23, pp. 1753–1759, 2007.
- [77] M. Gameiro, Y. Hiraoka, S. Izumi, M. Kramar, K. Mischaikow, and V. Nanda, “Topological measurement of protein compressibility via persistence diagrams,” *Japan Journal of Industrial and Applied Mathematics*, vol. 32, pp. 1–17, 2014.
- [78] Y. Dabaghian, F. Memoli, L. Frank, and G. Carlsson, “A topological paradigm for hippocampal spatial map formation using persistent homology,” *PLoS Comput Biol*, vol. 8, p. e1002581, 08 2012.
- [79] J. A. Perea, A. Deckard, S. B. Haase, and J. Harer, “Sw1pers: Sliding windows and 1-persistence scoring; discovering periodicity in gene expression time series data,” *BMC Bioinformatics*, vol. 16, p. 257, 2015.

- [80] B. Krishnamoorthy, S. Provan, and A. Tropsha, "A topological characterization of protein structure," in *Data Mining in Biomedicine, Springer Optimization and Its Applications*, pp. 431–455, 2007.
- [81] Y. Yao, J. Sun, X. H. Huang, G. R. Bowman, G. Singh, M. Lesnick, L. J. Guibas, V. S. Pande, and G. Carlsson, "Topological methods for exploring low-density states in biomolecular folding pathways," *The Journal of Chemical Physics*, vol. 130, p. 144115, 2009.
- [82] H. W. Chang, S. Bacallado, V. S. Pande, and G. E. Carlsson, "Persistent topology and metastable state in conformational dynamics," *PLoS ONE*, vol. 8, no. 4, p. e58699, 2013.
- [83] S. Biasotti, L. De Floriani, B. Falcidieno, P. Frosini, D. Giorgi, C. Landi, L. Papaleo, and M. Spagnuolo, "Describing shapes by geometrical-topological properties of real functions," *ACM Computing Surveys*, vol. 40, no. 4, p. 12, 2008.
- [84] J. Bennett, F. Vivodtzev, and V. Pascucci, eds., *Topological and statistical methods for complex data: Tackling large-scale, high-dimensional and multivariate data spaces*. Mathematics and Visualization, Springer-Verlag Berlin Heidelberg, 2015.
- [85] P. T. Bremer, V. P. I. Hotz, and R. Peikert, eds., *Topological methods in data analysis and visualization III: Theory, algorithms and applications*. Mathematics and Visualization, Springer International Publishing, 2014.
- [86] I. Fujishiro, Y. Takeshima, T. Azuma, and S. Takahashi, "Volume data mining using 3d field topology analysis," *IEEE Computer Graphics and Applications*, vol. 20, no. 5, pp. 46–51, 2000.
- [87] K. L. Xia, X. Feng, Y. Y. Tong, and G. W. Wei, "Persistent homology for the quantitative prediction of fullerene stability," *Journal of Computational Chemistry*, vol. 36, pp. 408–422, 2015.
- [88] B. Wang and G. W. Wei, "Object-oriented persistent homology," *Journal of Computational Physics*, vol. 305, pp. 276–299, 2016.
- [89] K. L. Xia, Z. X. Zhao, and G. W. Wei, "Multiresolution topological simplification," *Journal Computational Biology*, vol. 22, pp. 1–5, 2015.
- [90] K. L. Xia, Z. X. Zhao, and G. W. Wei, "Multiresolution persistent homology for excessively large biomolecular datasets," *Journal of Chemical Physics*, vol. 143, p. 134103, 2015.
- [91] K. L. Xia and G. W. Wei, "Persistent topology for cryo-EM data analysis," *International Journal for Numerical Methods in Biomedical Engineering*, vol. 31, p. e02719, 2015.
- [92] Z. X. Cang, L. Mu, K. Wu, K. Opron, K. Xia, and G.-W. Wei, "A topological approach to protein classification," *Molecular based Mathematical Biologys*, vol. 3, pp. 140–162, 2015.
- [93] B. Liu, B. Wang, R. Zhao, Y. Tong, and G. W. Wei, "ESES: software for Eulerian solvent excluded surface," *Journal of Computational Chemistry*, vol. 38, pp. 446–466, 2017.
- [94] Z. X. Cang and G. W. Wei, "TopologyNet: Topology based deep convolutional neural networks for biomolecular property predictions," *Plos Computational Biology*, Accepted, 2017.
- [95] D. Cohen-Steiner, H. Edelsbrunner, J. Harer, and Y. Mileyko, "Lipschitz functions have L_p -stable persistence," *Foundations of computational mathematics*, vol. 10, no. 2, pp. 127–139, 2010.
- [96] G. Carlsson, "Topological pattern recognition for point cloud data," *Acta Numerica*, vol. 23, pp. 289–368, 2014.
- [97] Z. Liu, Y. Li, L. Han, J. Liu, Z. Zhao, W. Nie, Y. Liu, and R. Wang, "PDB-wide collection of binding data: current status of the PDBbind database," *Bioinformatics*, vol. 31, no. 3, pp. 405–412, 2015.
- [98] P. M. Kasson, A. Zomorodian, S. Park, N. Singhal, L. J. Guibas, and V. S. Pande, "Persistent voids: a new structural metric for membrane fusion," *Bioinformatics*, vol. 23, no. 14, pp. 1753–1759, 2007.

- [99] K. L. Xia and G. W. Wei, "Multidimensional persistence in biomolecular data," *Journal Computational Chemistry*, vol. 36, pp. 1502–1520, 2015.
- [100] M. A. Miteva, F. Guyon, and P. Tufféry, "Frog2: Efficient 3d conformation ensemble generator for small compounds," *Nucleic acids research*, vol. 38, no. suppl 2, pp. W622–W627, 2010.
- [101] D. D. Nguyen, T. Xiao, M. L. Wang, and G. W. Wei, "Rigidity strengthening: A mechanism for protein-ligand binding," *Journal of Chemical Information and Modeling*, in press, 2017.
- [102] K. L. Xia, K. Opron, and G. W. Wei, "Multiscale multiphysics and multidomain models — Flexibility and rigidity," *Journal of Chemical Physics*, vol. 139, p. 194109, 2013.
- [103] D. Cohen-Steiner, H. Edelsbrunner, and J. Harer, "Stability of persistence diagrams," in *Proceedings of the twenty-first annual symposium on Computational geometry*, pp. 263–271, ACM, 2005.
- [104] D. Burago, Y. Burago, and S. Ivanov, *A course in metric geometry*, vol. 33. American Mathematical Society Providence, RI, 2001.
- [105] K. Tian, X. Yang, Q. Kong, C. Yin, R. L. He, and S. S.-T. Yau, "Two dimensional yau-hausdorff distance with applications on comparison of dna and protein sequences," *PLoS one*, vol. 10, no. 9, p. e0136577, 2015.
- [106] F. Pedregosa, G. Varoquaux, A. Gramfort, V. Michel, B. Thirion, O. Grisel, M. Blondel, P. Prettenhofer, R. Weiss, V. Dubourg, J. Vanderplas, A. Passos, D. Cournapeau, M. Brucher, M. Perrot, and E. Duchesnay, "Scikit-learn: Machine learning in Python," *Journal of Machine Learning Research*, vol. 12, pp. 2825–2830, 2011.
- [107] F. Chollet, "Keras." <https://github.com/fchollet/keras>, 2015.
- [108] Theano Development Team, "Theano: A Python framework for fast computation of mathematical expressions," *arXiv e-prints*, vol. abs/1605.02688, May 2016.
- [109] J. C. Pereira, E. R. Caffarena, and C. d. Santos, "Boosting docking-based virtual screening with deep learning," *arXiv preprint arXiv:1608.04844*, 2016.
- [110] J. D. Durrant, A. J. Friedman, K. E. Rogers, and J. A. McCammon, "Comparing neural-network scoring functions and the state of the art: applications to common library screening," *Journal of chemical information and modeling*, vol. 53, no. 7, pp. 1726–1735, 2013.
- [111] M. Arciniega and O. F. Lange, "Improvement of virtual screening results by docking data feature analysis," *Journal of chemical information and modeling*, vol. 54, no. 5, pp. 1401–1411, 2014.
- [112] B. Wang, Z. Zhao, D. D. Nguyen, and G. W. Wei, "Feature functional theory - binding predictor (FFT-BP) for the blind prediction of binding free energy," *Theoretical Chemistry Accounts*, vol. 136, p. 55, 2017.
- [113] T. Cheng, X. Li, Y. Li, Z. Liu, and R. Wang, "Comparative assessment of scoring functions on a diverse test set," *J. Chem. Inf. Model.*, vol. 49, pp. 1079–1093, 2009.
- [114] H. M. Berman, J. Westbrook, Z. Feng, G. Gilliland, T. N. Bhat, H. Weissig, I. N. Shindyalov, and P. E. Bourne, "The protein data bank," *Nucleic acids research*, vol. 28, no. 1, pp. 35–242, 2000.
- [115] H. Li, K.-S. Leung, M.-H. Wong, and P. J. Ballester, "Improving autodock vina using random forest: the growing accuracy of binding affinity prediction by the effective exploitation of larger data sets," *Molecular Informatics*, vol. 34, no. 2-3, pp. 115–126, 2015.
- [116] H. Li, K.-S. Leung, M.-H. Wong, and P. J. Ballester, "Low-Quality Structural and Interaction Data Improves Binding Affinity Prediction via Random Forest," *Molecules*, vol. 20, pp. 10947–10962, 2015.
- [117] N. Huang, B. K. Shoichet, and J. J. Irwin, "Benchmarking sets for molecular docking," *Journal of medicinal chemistry*, vol. 49, no. 23, pp. 6789–6801, 2006.

- [118] M. M. Mysinger and B. K. Shoichet, "Rapid context-dependent ligand desolvation in molecular docking," *Journal of chemical information and modeling*, vol. 50, no. 9, pp. 1561–1573, 2010.
- [119] J. J. Irwin and B. K. Shoichet, "Zinc- a free database of commercially available compounds for virtual screening," *Journal of chemical information and modeling*, vol. 45, no. 1, pp. 177–182, 2005.
- [120] M. S. Armstrong, G. M. Morris, P. W. Finn, R. Sharma, L. Moretti, R. I. Cooper, and W. G. Richards, "Electroshape: fast molecular similarity calculations incorporating shape, chirality and electrostatics," *Journal of computer-aided molecular design*, vol. 24, no. 9, pp. 789–801, 2010.
- [121] Z. Xiang and B. Honig, "Extending the accuracy limits of prediction for side-chain conformations," *J Mol Biol*, vol. 311, no. 2, pp. 421–430–405, 2001.
- [122] G. M. Morris, R. Huey, W. Lindstrom, M. F. Sanner, R. K. Belew, D. S. Goodsell, and A. J. Olson, "Autodock4 and autodocktools4: Automated docking with selective receptor flexibility," *Journal of computational chemistry*, vol. 30, no. 16, pp. 2785–2791, 2009.
- [123] O. Trott and A. J. Olson, "AutoDock Vina: improving the speed and accuracy of docking with a new scoring function, efficient optimization, and multithreading," *J Computat Chem*, vol. 31, no. 2, pp. 455–461, 2010.
- [124] M. A. Neves, M. Totrov, and R. Abagyan, "Docking and scoring with icm: the benchmarking results and strategies for improvement," *Journal of computer-aided molecular design*, vol. 26, no. 6, pp. 675–686, 2012.
- [125] J. B. Cross, D. C. Thompson, B. K. Rai, J. C. Baber, K. Y. Fan, Y. Hu, and C. Humblet, "Comparison of several molecular docking programs: pose prediction and virtual screening accuracy," *Journal of chemical information and modeling*, vol. 49, no. 6, pp. 1455–1474, 2009.